Article

Neuron

Npas4 Is a Critical Regulator of Learning-Induced Plasticity at Mossy Fiber-CA3 Synapses during Contextual Memory Formation

Highlights

- Npas4 selectively restricts the number of MF-CA3 synaptic contacts
- Contextual learning selectively strengthens MF inputs on CA3 pyramidal neurons
- Npas4 deletion prevents learning-induced strengthening of MF inputs
- PIK2 functions downstream of Npas4 to modulate MF-CA3 synapses

Authors

Feng-Ju Weng, Rodrigo I. Garcia, Stefano Lutzu, ..., Kwanghun Chung, Pablo E. Castillo, Yingxi Lin

Correspondence

yingxi@mit.edu

In Brief

Weng et al. report that the transcription factor Npas4 selectively regulates the number of functional synaptic contacts between CA3 pyramidal neurons and mossy fibers, allowing for learning-induced modification of MF-CA3 synapses during contextual memory formation.

Weng et al., 2018, Neuron *97*, 1–16
March 7, 2018
https://doi.org/10.1016/j.neuron.2018.01.026

CellPress

Please cite this article in press as: Weng et al., Npas4 Is a Critical Regulator of Learning-Induced Plasticity at Mossy Fiber-CA3 Synapses during Contextual Memory Formation, Neuron (2018), https://doi.org/10.1016/j.neuron.2018.01.026

Neuron
Article

Npas4 Is a Critical Regulator of Learning-Induced Plasticity at Mossy Fiber-CA3 Synapses during Contextual Memory Formation

Feng-Ju Weng,[1] Rodrigo I. Garcia,[1] Stefano Lutzu,[2] Karina Alviña,[2,7] Yuxiang Zhang,[1] Margaret Dushko,[1] Taeyun Ku,[3,4] Khaled Zemoura,[3] David Rich,[1] Dario Garcia-Dominguez,[1] Matthew Hung,[1] Tushar D. Yelhekar,[1] Andreas Toft Sørensen,[1,8] Weifeng Xu,[3] Kwanghun Chung,[3,4,5,6] Pablo E. Castillo,[2] and Yingxi Lin[1,9,*]

[1]McGovern Institute for Brain Research, Department of Brain and Cognitive Sciences, Massachusetts Institute of Technology (MIT), Cambridge, MA, USA
[2]Dominick P. Purpura Department of Neuroscience, Albert Einstein College of Medicine, Bronx, NY, USA
[3]Picower Institute for Learning and Memory, Department of Brain and Cognitive Sciences, MIT, Cambridge, MA, USA
[4]Institute for Medical Engineering and Science, MIT, Cambridge, MA, USA
[5]Department of Chemical Engineering, MIT, Cambridge, MA, USA
[6]Harvard-MIT Division of Health Sciences and Technology, MIT, Cambridge, MA, USA
[7]Present address: Department of Biological Sciences, Texas Tech University, Lubbock, TX, USA
[8]Present address: Department of Neuroscience, University of Copenhagen, Copenhagen, Denmark
[9]Lead Contact
*Correspondence: yingxi@mit.edu
https://doi.org/10.1016/j.neuron.2018.01.026

SUMMARY

Synaptic connections between hippocampal mossy fibers (MFs) and CA3 pyramidal neurons are essential for contextual memory encoding, but the molecular mechanisms regulating MF-CA3 synapses during memory formation and the exact nature of this regulation are poorly understood. Here we report that the activity-dependent transcription factor Npas4 selectively regulates the structure and strength of MF-CA3 synapses by restricting the number of their functional synaptic contacts without affecting the other synaptic inputs onto CA3 pyramidal neurons. Using an activity-dependent reporter, we identified CA3 pyramidal cells that were activated by contextual learning and found that MF inputs on these cells were selectively strengthened. Deletion of Npas4 prevented both contextual memory formation and this learning-induced synaptic modification. We further show that Npas4 regulates MF-CA3 synapses by controlling the expression of the polo-like kinase Plk2. Thus, Npas4 is a critical regulator of experience-dependent, structural, and functional plasticity at MF-CA3 synapses during contextual memory formation.

INTRODUCTION

The hippocampus is critical for contextual memory formation, and specific synaptic connections within this region carry out the neuronal computations required for encoding, storing, and retrieving contextual memories (Kesner and Rolls, 2015). Contextual information that flows from the entorhinal cortex (EC) into the hippocampus is processed through the trisynaptic loop formed by three interconnected but anatomically and functionally distinct sub-regions: the dentate gyrus (DG), *cornu ammonis 3* (CA3), and CA1. At the center of the trisynaptic loop, pyramidal neurons in CA3 receive three major excitatory synaptic inputs: mossy fiber (MF) inputs from DG granule cells, perforant path inputs directly from the EC, and recurrent inputs from other CA3 pyramidal neurons. Computational models predict that the MF-CA3 connections are essential for encoding new contextual memory but are dispensable for contextual memory retrieval, which, instead, requires the perforant path (Treves and Rolls, 1992). Behavioral studies in which the DG was lesioned or MF transmission was pharmacologically inhibited support these theoretical predictions (Jerman et al., 2006; Lassalle et al., 2000; Lee and Kesner, 2004a, 2004b). However, the molecular mechanisms that regulate MF-CA3 synapses during memory formation and the exact nature of this regulation are currently unknown.

MF-CA3 synapses have several unique structural and functional properties. They are located on proximal dendrites of CA3 pyramidal neurons, have large presynaptic MF terminals (MFTs) with multiple release sites (Amaral and Dent, 1981) that make contact with large multi-headed postsynaptic spines (Chicurel and Harris, 1992) called complex spines or thorny excrescences (TEs), and display uniquely robust frequency facilitation (Salin et al., 1996). MF-CA3 synapses can act as "detonator" synapses; that is, under certain circumstances, a single MF input can reliably cause action potential firing of CA3 pyramidal neurons (Henze et al., 2002; Urban et al., 2001; Vyleta et al., 2016). In addition, MF-CA3 synapses exhibit dramatic structural plasticity at both presynaptic MFTs and postsynaptic TEs (Wiera and Mozrzymas, 2015). Both structures are readily modified by learning, stress, and aging (Galimberti et al., 2006; Gogolla et al., 2009; Magariños et al., 1997; Maruo et al., 2016; Rekart et al., 2007; Sandi et al., 2003) and are particularly sensitive to changes in levels of activity within the hippocampus (Ben-Ari and Represa,

1990; Chierzi et al., 2012; Kim and Tsien, 2008; Lee et al., 2013; Represa and Ben-Ari, 1992a, 1992b; Zhao et al., 2012b). Furthermore, these structural changes are correlated with functional changes, with larger morphology typically being associated with more numerous and stronger synaptic contacts between MFTs and TEs (Galimberti et al., 2006; Zhao et al., 2012a).

Long-term memory formation is believed to involve modifications in relevant neural circuits that likely occur as a result of enduring synaptic changes (Mayford et al., 2012). Although it is well established that the contextual information entering CA3 through the MF pathway is critical for the encoding of contextual memory in CA3 (Lee and Kesner, 2004a, 2004b; Rolls, 1996), and there is an abundance of evidence that MF-CA3 synapses are modified by experience (Galimberti et al., 2006; Gogolla et al., 2009; Magariños et al., 1997; Maruo et al., 2016; Rekart et al., 2007; Sandi et al., 2003), precisely how MF-CA3 synapses are modified to contribute to contextual memory formation remains an open question. While mechanistically diverse forms of synaptic plasticity have been identified at MF-CA3 synapses, most studies have focused on presynaptic plasticity, such as classical, NMDA receptor (NMDAR)-independent long-term potentiation (LTP) (Nicoll and Schmitz, 2005). Intriguingly, MF-LTP appears to be dispensable for encoding contextual memory (Ruediger et al., 2011), and it remains unclear what types of experience-dependent MF-CA3 synapse plasticity are involved in contextual learning. Moreover, molecular pathways responsible for the activity-dependent modulation of MF-CA3 synapses and the precise role of such modulation in contextual learning are poorly understood.

We have previously shown that the neuronal activity-dependent transcription factor Npas4 is required in CA3, but not in CA1, for hippocampus-dependent contextual memory formation (Ramamoorthi et al., 2011), based on the following evidence. After contextual learning, Npas4 is specifically induced in CA3 but not in CA1. Either global knockout or selective deletion of Npas4 in CA3 results in impaired contextual memory, and restoration of Npas4 in CA3 is sufficient to rescue the learning deficit in global knockout mice. In contrast, similar manipulations of Npas4 in CA1 had no effect on contextual memory. Here we report that Npas4 selectively regulates the structure and strength of MF-CA3 synapses. We also found that contextual learning selectively strengthens MF inputs on learning-activated CA3 pyramidal neurons. Deletion of Npas4 prevents this learning-induced plasticity at MF-CA3 synapses, which likely contributes to the impaired contextual memory formation. We further show that Npas4 acts through its transcriptional target polo-like kinase 2 (Plk2) to modulate MF-CA3 synapses. Expression of Plk2 in CA3 is sufficient to restore the MF-CA3 synapses and contextual memory formation in Npas4 global knockout mice. Thus, Npas4 emerges as a critical regulator of experience-dependent plasticity at MF-CA3 synapses during contextual memory formation.

RESULTS

Excitatory Synapses on CA3 Pyramidal Neurons Are Selectively Regulated by Npas4

To better understand the role of Npas4 in contextual memory, we first examined miniature excitatory and inhibitory postsynaptic currents (mEPSCs and mIPSCs, respectively) by performing whole-cell patch recordings in CA3 and CA1 pyramidal neurons of acute hippocampal slices from Npas4 knockout (KO) mice and their wild-type littermates. We used 8- to 10-week-old mice, the same age at which we found that Npas4 is required in CA3 for contextual memory formation (Ramamoorthi et al., 2011). We observed a robust increase in mEPSC frequency and amplitude in CA3 pyramidal neurons of Npas4 KO mice compared with their wild-type littermates (Figure 1A). In contrast, mEPSCs were unchanged in CA1 pyramidal neurons (Figure 1B). In addition, mIPSCs remained unchanged in Npas4 KO mice in both CA3 and CA1 pyramidal neurons (Figures 1C and 1D). Thus, Npas4 deletion is associated with a selective increase in excitatory miniature transmission on CA3 pyramidal neurons.

To rule out the possibility that the increase in excitatory drive on CA3 was a result of developmental compensation for global germline loss of Npas4, we acutely removed Npas4 by stereotaxic injection of adeno-associated virus AAV-hSyn-Cre-GFP (AAV-Cre) into the CA3 or CA1 region of Npas4 conditional KO (cKO; $Npas4^{flx/flx}$) mice, with AAV-hSyn-GFP (AAV-GFP) as a control. Miniature activity was measured from CA3 and CA1 pyramidal neurons in acute hippocampal slices prepared 3 days after viral injection, when we had confirmed that the Npas4 gene had been deleted (Figures 2A and 2B). As in the germline KO, mEPSC frequency in CA3 pyramidal neurons was increased more than 50% by Npas4 deletion compared with the GFP control condition (Figure 2C). In contrast, mEPSC amplitude was not affected in cKO mice, suggesting that Npas4 does not directly regulate the mEPSC amplitude. mEPSCs in CA1 pyramidal neurons (Figure 2D) and mIPSCs in CA3 pyramidal neurons (Figure S1) were again unchanged by Npas4 deletion. Taken together, our findings indicate that Npas4 selectively modulates the excitatory synaptic drive onto CA3 pyramidal neurons.

An abnormally elevated excitatory drive onto CA3 could be at least partly responsible for the impaired contextual memory we observed in Npas4-deficient animals (Ramamoorthi et al., 2011). If so, then re-expression of Npas4 in CA3 of Npas4 KO mice, a manipulation that rescued the deficit in contextual memory formation (Ramamoorthi et al., 2011), should also restore CA3 excitatory synaptic transmission to a normal level. Indeed, 3 days after a herpes simplex virus (HSV) encoding Npas4 was stereotaxically injected into CA3 of Npas4 KO mice, the mEPSC frequency in infected CA3 pyramidal neurons was reduced almost to the level seen in wild-type mice (Figures 2E–2G). Expression of GFP or a truncated, transcriptionally inactive form of Npas4 (ΔNpas4), neither of which rescued the learning and memory deficit (Ramamoorthi et al., 2011), failed to restore mEPSC activity (Figure 2G). mEPSC amplitudes were similar in all experiments. These results suggest that the increase in excitatory inputs onto CA3 pyramidal neurons by Npas4 deletion interferes with contextual memory formation.

Npas4 Selectively Regulates the MF Inputs on CA3 Pyramidal Neurons

We considered the possibility that Npas4 might selectively regulate a specific subset of the three types of synaptic inputs received by CA3 pyramidal neurons; i.e., MF, recurrent, or perforant path inputs. We have previously shown that deletion of

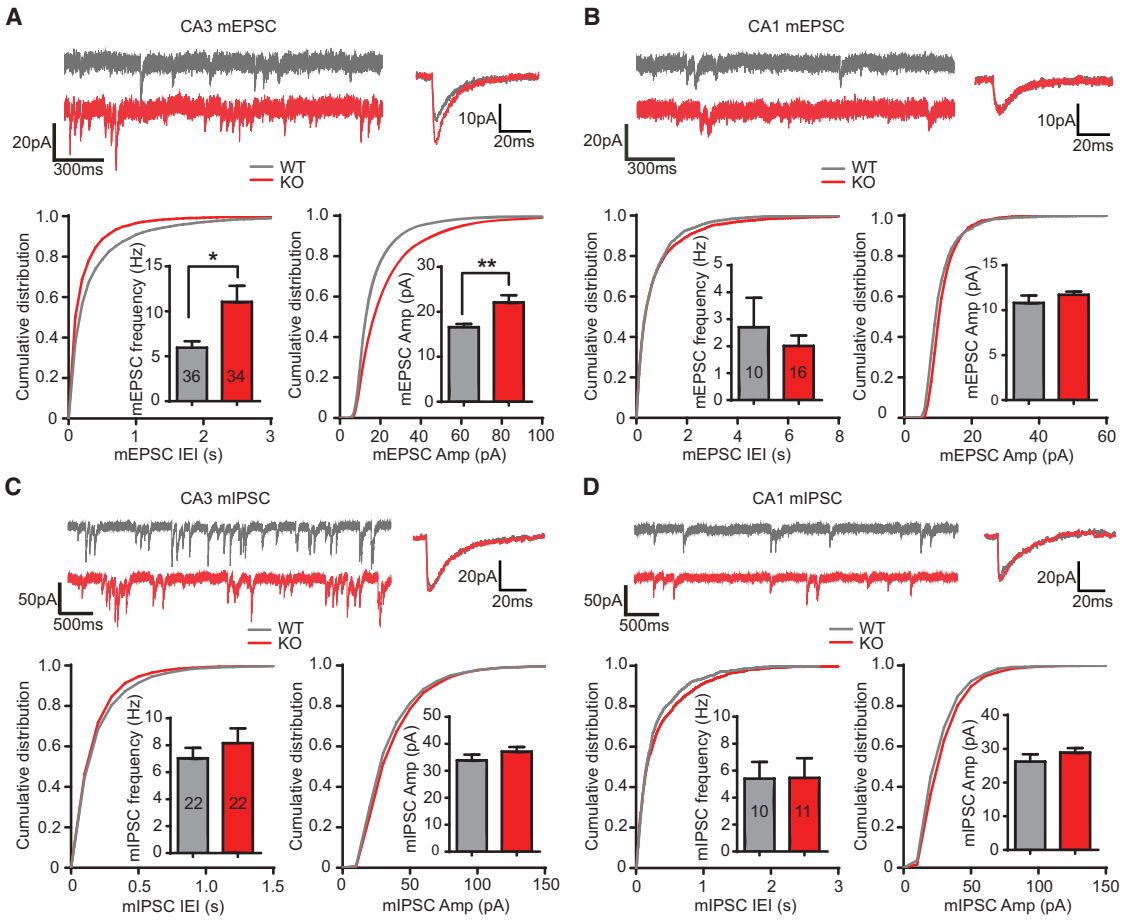

Figure 1. Excitatory Miniature Activity in CA3 but Not CA1 Pyramidal Neurons Is Significantly Increased in Npas4 KO Mice, whereas Inhibitory Miniature Activity Is Not Affected

(A) Sample traces (top left, raw traces; top right, average mEPSCs), summary bar graphs, and cumulative distribution of mEPSCs recorded from hippocampal CA3 pyramidal neurons. Frequency: wild-type (WT), 5.95 ± 0.71 Hz; KO, 11.05 ± 1.72 Hz; p = 0.043. Amplitude: WT, 16.61 ± 0.70 pA; KO, 22.12 ± 1.59 pA; p = 0.002. WT: n = 36 cells, 6 animals; KO: n = 34 cells, 5 animals.

(B) The same as (A) but for CA1 pyramidal neurons. Frequency: WT, 2.70 ± 1.09 Hz; KO, 2.01 ± 0.38 Hz; p = 0.85. Amplitude: WT, 10.82 ± 0.82 pA; KO, 11.72 ± 0.35 pA; p = 0.15. WT, n = 10 cells, 3 animals; KO, n = 16 cells, 3 animals.

(C) Sample traces, summary bar graphs, and cumulative distribution of mIPSC recorded from hippocampal CA3 neurons. Frequency: WT, 7.04 ± 0.77 Hz; KO, 8.16 ± 1.09 Hz; p = 0.37. Amplitude: WT, 33.91 ± 2.10 pA; KO, 37.14 ± 1.67 pA; p = 0.14. WT: n = 22 cells, 3 animals; KO: n = 22 cells, 4 animals.

(D) The same as (C) but for CA1 pyramidal neurons. Frequency: WT, 5.41 ± 1.23 Hz; KO, 5.47 ± 1.46 Hz; p = 0.74. Amplitude: WT, 26.24 ± 2.13 pA; KO, 28.92 ± 1.32 pA; p = 0.22. WT: n = 10 cells, 3 animals; KO: n = 11 cells, 3 animals.

Data are shown as mean ± SEM. *p < 0.05, **p < 0.01, Mann-Whitney *U* test.

Npas4 in CA3 does not affect short-term memory formation (Ramamoorthi et al., 2011), a process likely depending on recurrent inputs from other CA3 neurons (Kesner, 2007). Contextual memory encoding and retrieval depend on MF and perforant path inputs, respectively (Jerman et al., 2006; Lassalle et al., 2000; Lee and Kesner, 2004a). Because deletion of Npas4 in CA3 before contextual fear conditioning (CFC) training impairs formation of long-term contextual memory (Ramamoorthi et al., 2011), it suggests that Npas4 could be involved in either encoding or retrieval of contextual memory or both. We next investigated whether Npas4 could be selectively involved in memory encoding or retrieval. Npas4 cKO mice were subjected to CFC training, and their contextual memory was examined the following day by re-exposing them to the same context (recall 1, Figure 3A). One day later, the animals were injected in CA3 with AAV-Cre to delete Npas4 or with AAV-GFP as a control. Three days after injection, their contextual memory was examined again (recall 2). We found that the levels of freezing behavior were similar at recall 1 and recall 2 for all mice, regardless of whether Npas4 was deleted (Figures 3A and 3B). This result, combined with our previous findings (Ramamoorthi et al., 2011), indicates that Npas4 is required in CA3 for memory encoding but not retrieval, in agreement with the notion that Npas4 modulates MF-CA3 synapses and not the perforant path.

Consistent with the idea that Npas4 selectively modulates MF-CA3 synapses, we found that a significantly large fraction

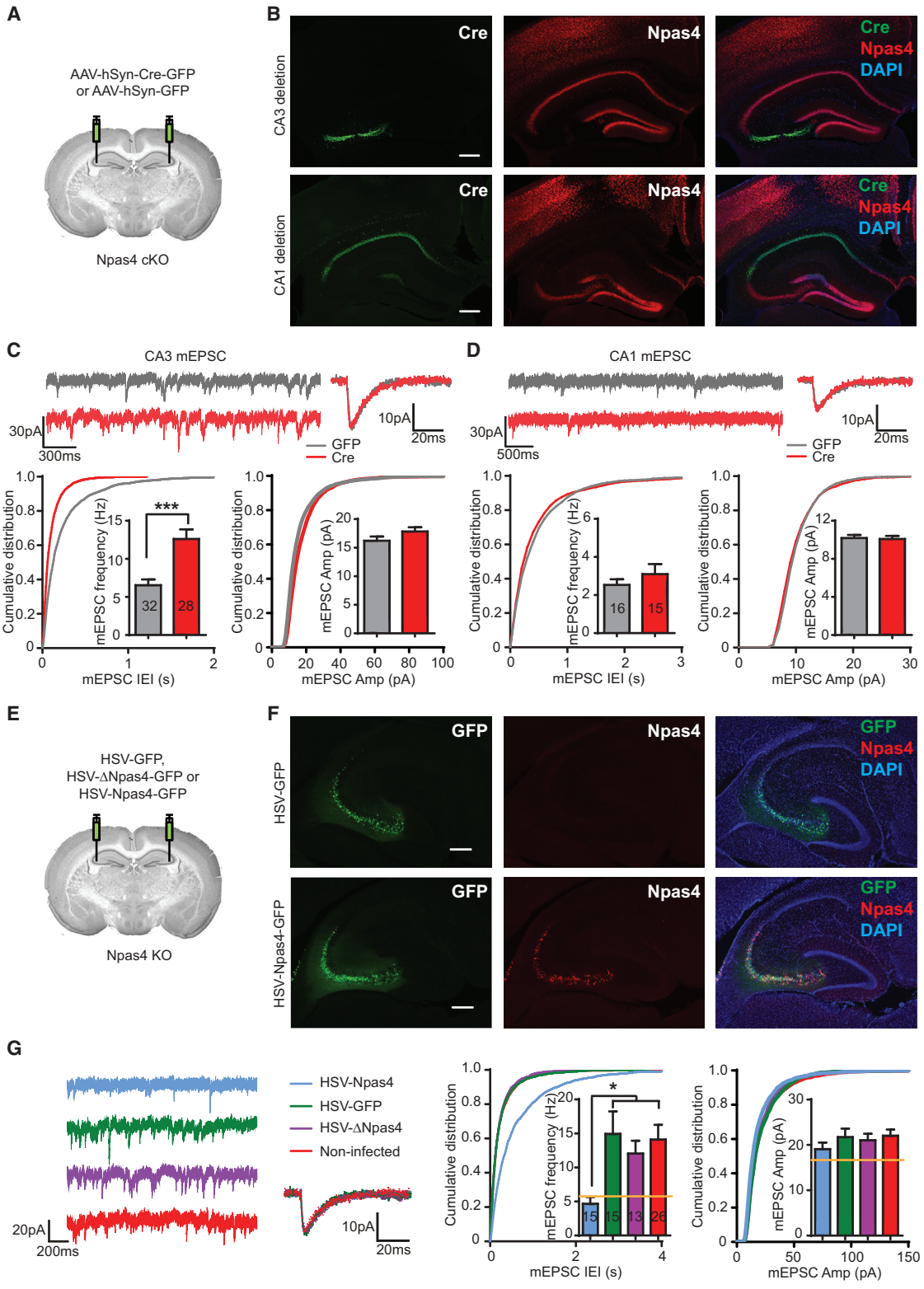

Figure 2. The mEPSC Frequency in CA3 Pyramidal Neurons Is Significantly Altered by Acute Manipulation of Npas4 Expression

(A) AAV1-hSyn-Cre-EGFP (Cre) or AAV1-hSyn-EGFP (GFP) was stereotaxically injected into the CA3 or CA1 region of Npas4$^{flx/flx}$ mice at 8–10 weeks of age. Whole-cell voltage-clamp recordings were performed 3 days after virus injection.

(legend continued on next page)

of mEPSC events with short rise times (<2.5 ms) in the Npas4 KO CA3 neurons (Figure S2), as expected for events, originated close to the cell soma, like those generated by MF-CA3 synapses (Claiborne et al., 1993; Jonas et al., 1993). Moreover, the elevated mEPSC activity observed in Npas4-deficient neurons (Figure 2C) was abolished in the presence of the metabotropic glutamate receptor subtype 2/3 (mGluR2/3)-specific agonist DCG-IV (1 μM) (Figure 3C), a manipulation known to specifically suppress glutamate release from MFs but not recurrent or perforant path inputs (Kamiya and Ozawa, 1999; Kamiya et al., 1996). Furthermore, using minimal stimulation of MF inputs (Figure S3; Hofmann et al., 2008; Jonas et al., 1993), we found that MF-CA3 synaptic efficacy was increased in Npas4 KO mice compared with their wild-type littermates and that this enhancement was associated with increased potency but no change in failure rate (Figures 3D and 3E). In addition, paired-pulse ratio (PPR) and burst-induced facilitation of evoked MF-CA3 synaptic responses, two forms of short-term synaptic plasticity that are inversely correlated with the probability of neurotransmitter release (Pr), were undistinguishable in Npas4 KO and wild-type littermates (Figure 3F). Classical presynaptic LTP at MF-CA3 synapses was also normal in Npas4 KO mice (Figure 3G). Taken together, our results therefore suggest that the selective increase in MF-CA3 transmission observed in Npas4-deficient neurons likely results from an increase in the number of functional synaptic contacts established by each MF. In contrast, Npas4 deletion does not affect MF-CA3 basal Pr or classical forms of presynaptic plasticity.

Npas4 Selectively Restricts the Number of MF-CA3 Synaptic Contacts

The number of conventional glutamatergic synapses on pyramidal neurons is correlated with the density of dendritic spines (Alvarez and Sabatini, 2007; Yuste and Bonhoeffer, 2001). To test whether changes in the number of MF-CA3 synaptic contacts is correlated with morphological changes, we designed a strategy to sparsely and brightly label MF terminals and TEs in different colors using DNA recombinase Flp°-dependent reporters expressing both cytosolic and membrane-bound farnesylated GFP (AAV-hSyn-fDIO-GFP-P2A-^{farn}GFP) or tdTomato (AAV-hSyn-fDIO-tdTomato) (Figure 4A; see STAR Methods for details). We performed bilateral double injections on Npas4 cKO mice. One injection, targeting dorsal CA3, delivered AAV-hSyn-Cre-GFP (to delete Npas4) or AAV-hSyn-ΔCre-GFP (containing a truncated and inactive version of Cre as the control), low-titer AAV-EF1α-Flp° (for sparse labeling), and AAV-hSyn-fDIO-tdTomato. This resulted in nuclear GFP labeling of the majority of dorsal CA3 neurons by either Cre-GFP or ΔCre-GFP and a sparse population of CA3 neurons labeled red by tdTomato (Figures 4A and 4B). A second injection was targeted to the dorsal DG, delivering low-titer AAV-EF1α-Flp° and AAV-hSyn-fDIO-GFP-P2A-^{farn}GFP to label MFTs in green (Figures 4A and 4B).

To analyze the 3D structures of MFTs and TEs, we adopted the See Deep Brain 2 (SeeDB2) procedure to immuno-stain and clarify brain slices for confocal imaging (Ke et al., 2016). SeeDB2 appears to be superior to other tissue-clearing procedures in preserving synaptic ultrastructure such as dendritic spines (K.Z. and W.X., unpublished observation). The 3D structures of MF terminals and TEs were reconstructed and their total volumes quantified (Figures 4C–4F). We found that deletion of Npas4 in CA3 results in significantly larger MFT and TE structures (Figures 4G and 4H), supporting our hypothesis that loss of Npas4 increases the number of synaptic contacts between MFTs and TEs.

To unequivocally determine that Npas4 deletion in CA3 increases the total number of MF-CA3 synaptic contacts, as opposed to increasing the proportion of functional synapses, we examined the density of synapses within the *stratum lucidum*, where MF-CA3 synapses reside. We adopted a recently developed tissue processing technique called magnified analysis of proteome (MAP) (Ku et al., 2016). By combining tissue expansion, clarification, and immunostaining, MAP allows 3D analysis of the subcellular localization of individual synaptic components using a conventional confocal microscope (Figure 4I). We first measured densities within randomly selected cubic regions of the *stratum lucidum*. Npas4 deletion increased the densities of the pre-synaptic active zone marker Bassoon, the post-synaptic marker PSD-95, and the density of synapses defined by overlapped Bassoon and PSD-95 puncta, whereas the average sizes of the Bassoon and PSD-95 puncta remained unchanged (Figures 4J–4L). We also found that the density of synapses within individual MF terminals remained unchanged regardless of the

(B) Representative images showing complete Npas4 gene deletion from the CA3 (top) or CA1 (bottom) region in Npas4$^{flx/flx}$ mice 3 days after injection of Cre. Npas4 expression (red) following kainic acid-induced seizure was completely absent in regions expressing Cre (green). The scale bars correspond to 300 μm.
(C) Sample traces, summary bar graphs, and cumulative distribution of mEPSCs recorded from hippocampal CA3 pyramidal neurons from Npas4$^{flx/flx}$ mice injected with Cre or GFP. Frequency: GFP, 6.55 ± 0.75 Hz; Cre, 12.61 ± 1.26 Hz; p = 0.0002. Amplitude: GFP, 16.22 ± 0.73 pA; Cre, 17.83 ± 0.74 pA; p = 0.087. GFP: n = 32 cells, 6 animals; Cre: n = 28 cells, 6 animals.
(D) The same as (C) but for CA1 pyramidal neurons. Frequency: GFP, 2.53 ± 0.30 Hz; Cre, 3.10 ± 0.52 Hz; p = 0.68. Amplitude: GFP, 10.19 ± 0.32 pA; Cre, 10.09 ± 0.32 pA; p = 0.82. GFP: n = 16 cells, 4 animals; Cre: n = 15 cells, 3 animals.
(E) HSV-EGFP, HSV-Npas4-EGFP, or HSV-ΔNpas4-EGFP was stereotaxically injected into the CA3 region of Npas4 KO mice at 8–10 weeks of age. Whole-cell voltage-clamp recordings were performed 3 days after virus injection.
(F) Representative images showing acute re-expression of Npas4 in CA3 of Npas4 KO mice using HSV-Npas4-EGFP (bottom). HSV-EGFP was used as a control (top). The scale bars correspond to 300 μm.
(G) Sample traces, cumulative distribution, and summary bar graphs of mEPSCs recorded from hippocampal CA3 pyramidal cells of Npas4 KO mice after expression of Npas4, GFP, or ΔNpas4 or from uninfected cells. Horizontal lines indicate the levels in WT animals (from Figure 1A). Frequency: Npas4, 4.68 ± 0.98 Hz; GFP, 14.94 ± 3.30 Hz; ΔNpas4, 12.05 ± 1.88 Hz; uninfected, 14.10 ± 2.16 Hz; F (3, 65) = 3.739; p = 0.015. Amplitude: Npas4, 19.09 ± 1.43 pA; GFP, 21.75 ± 1.84 pA; ΔNpas4, 21.04 ± 1.43 pA; uninfected, 22.04 ± 1.36 pA; F (3, 65) = 0.7318; p = 0.54. Npas4: n = 15 cells, 3 animals; GFP: n = 15 cells, 3 animals; ΔNpas4: n = 13 cells, 3 animals; uninfected: n = 26 cells, 9 animals.
Data are shown as mean ± SEM. In (C) and (D), ***p < 0.001, Mann-Whitney *U* test. In (G), *p < 0.05, one-way ANOVA, Dunnett's post hoc test. See also Figure S1.

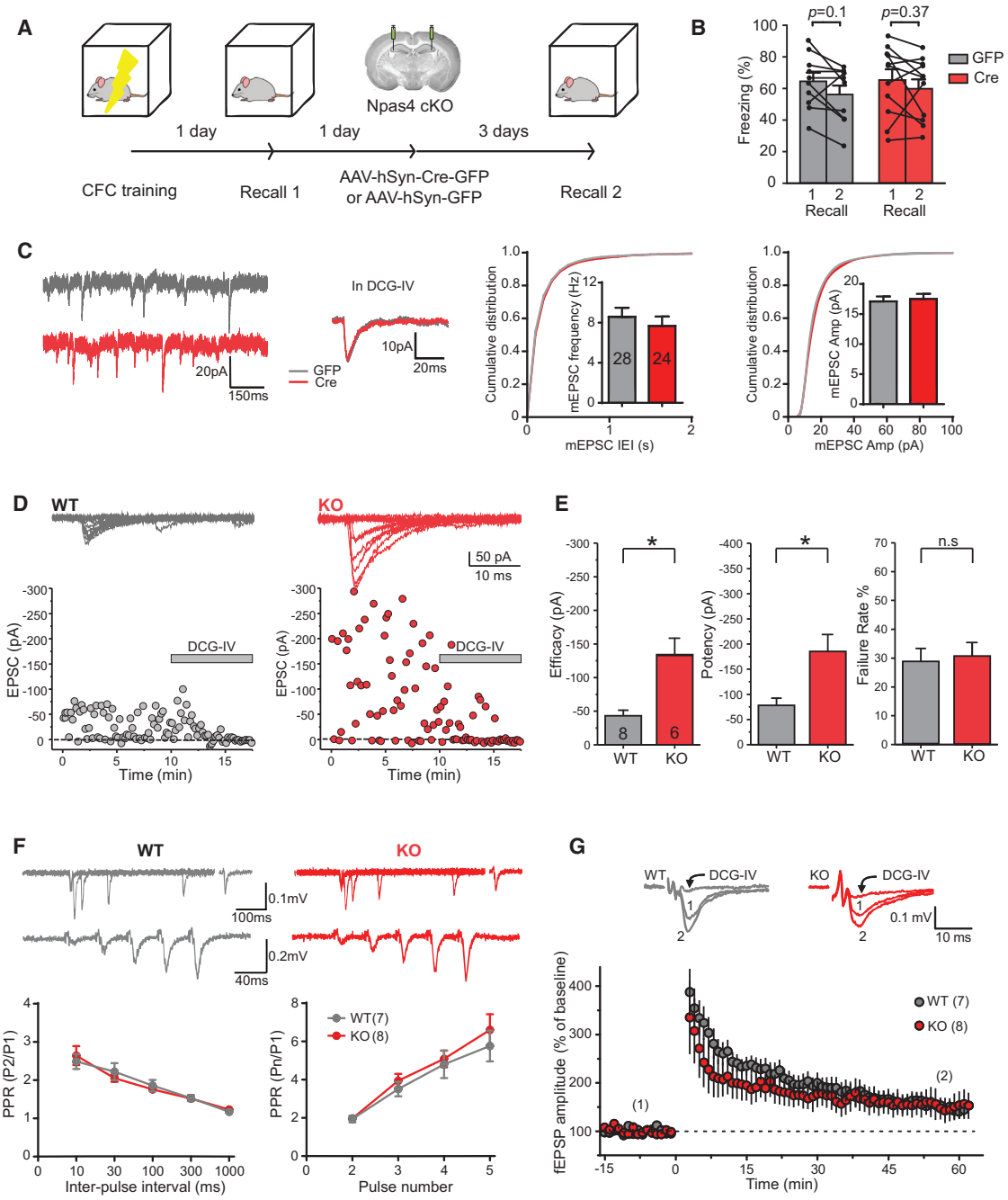

Figure 3. Deletion of Npas4 in CA3 Selectively Alters the Excitatory Inputs Received by CA3 Pyramidal Neurons from MFs, whereas Short-Term and Long-Term Plasticity Remains Unchanged

(A and B) Npas4 is not required in CA3 for retrieval of contextual memory.

(A) Npas4 cKO mice underwent CFC training, and their contextual memories were recalled the following day (recall 1). Npas4 was deleted 1 day after recall 1, and contextual memories were re-examined 3 days after surgery (recall 2).

(B) All animals, regardless of the presence or absence of Npas4, displayed similar freezing levels during both recalls. GFP freezing level: recall 1, 64.58% ± 5.22%; recall 2, 56.25% ± 5.35%; p = 0.1. Cre freezing level: recall 1, 65.34% ± 6.85%; recall 2, 59.85% ± 5.94%; p = 0.27. Wilcoxon matched pairs signed rank tests were used to compare recall 1 and recall 2 for each treatment.

(C) AAV1-hSyn-EGFP (GFP) or AAV1-hSyn-Cre-EGFP (Cre) was stereotaxically injected into the CA3 region of Npas4$^{flx/flx}$ mice at 8–10 weeks of age. Whole-cell voltage-clamp recordings were performed 3 days after virus injection. In the presence of 1 μM DCG-IV (to block MF transmission), Npas4 deletion had no effect on the frequency or amplitude of mEPSCs recorded from CA3 pyramidal neurons. Sample traces, summary bar graphs, and cumulative distributions are shown. Frequency: GFP, 8.60 ± 0.89 Hz; Cre, 7.68 ± 0.93 Hz; p = 0.46. Amplitude: GFP, 17.10 ± 0.82 pA; Cre, 17.53 ± 0.83 pA; p = 0.65. GFP: n = 28 cells, 7 animals; Cre: n = 24 cells, 7 animals.

(legend continued on next page)

presence of Npas4 (Figure 4M), suggesting that the enlargement of the synaptic structure in Npas4-deficient CA3 neurons is associated with an increase in synaptic contacts per MF terminal/TE and that this structural change likely underlies the increase in MF-CA3 synaptic transmission observed in the absence of Npas4.

A more conventional and higher-throughput 2D morphological analysis of TE size using the "stick and stain" method (Wallace and Bear, 2004) also showed a significant increase in TE size in both Npas4 KOs and cKOs (Figures 5A and 5B). In contrast, dendritic spine densities in apical and basal distal dendrites (i.e., more than 30 μm from the soma), where recurrent and perforant path inputs are found, were indistinguishable in Npas4 KO and the wild-type (Figure 5C), consistent with our electrophysiological findings indicating unchanged inputs from these two pathways (Figure 3E). Remarkably, expressing Npas4 in CA3 of Npas4 KO mice, which rescues the contextual learning deficit (Ramamoorthi et al., 2011) and restores changes in CA3 mEPSCs (Figures 2E–2G), reduced TE sizes to wild-type levels, whereas expressing the truncated, transcriptionally inactive form ΔNpas4 had no such effect (Figure 5D). Altogether, our data indicate that Npas4 selectively restricts the size of MFTs and TEs and the number of functional contacts between them.

Contextual Learning Selectively Strengthens MF Inputs on Learning-Activated CA3 Pyramidal Neurons

Given that Npas4 is required in CA3 for contextual memory formation (Ramamoorthi et al., 2011) and our new findings indicating that Npas4 selectively regulates MF-CA3 synapses, we hypothesized that these synapses are modulated during contextual memory formation. To identify synaptic changes directly associated with a contextual learning experience, we took advantage of our recently developed robust activity marking (RAM) system (Sørensen et al., 2016), which allows us to tag neurons selectively activated by CFC. The RAM system is composed of a synthetic promoter that is strongly activated by neuronal activity and a downstream reporter gene to allow subsequent investigation and manipulation (Figure 6A). A modified doxycycline (Dox)-dependent Tet-Off system provides the temporal control to label neurons that are activated by a specific experience, which occurs in the absence of Dox. We have recently shown that the RAM system selectively labels neuron ensembles activated by contextual learning in various brain regions, including CA3 (Sørensen et al., 2016).

In the process of developing the RAM system, we had previously found that CA3 neurons activated by exposure to an enriched environment (EE) and, hence, labeled by RAM (Figure S4A) have significantly higher mEPSC frequencies (Figure S4B) and a modest decrease in their mIPSC amplitude (Figure S4C). This result suggests that contextual learning may selectively strengthen MF-CA3 connections on the activated CA3 neurons and leads to the hypothesis that Npas4 deletion abolishes this learning-induced synaptic modification, leading to the observed impairment in contextual memory formation.

To identify neurons that are activated by CFC, we stereotaxically injected AAV-RAM-mKate2, which expresses the reporter gene mKate2 in activated neurons, into CA3 of wild-type C57BL/6 mice. The mice were then placed on a Dox diet for 5 days, switched to Dox-free food for 48 hr, and then subjected to CFC; mEPSC measurements were carried out 24 hr later (Figure 6B). CA3 neurons activated during CFC and, hence, labeled by mKate2 (RAM+) had a substantially higher mEPSC frequency than neighboring unlabeled (RAM−) pyramidal neurons (Figure 6C). This difference was abolished when mEPSC measurements were carried out in the presence of the selective mGluR2/3 agonist LY354740, which, like DCG-IV, blocks MF-CA3 transmission (Figure 6C). This result suggests that contextual learning selectively strengthens MF inputs onto the ensemble of CA3 neurons that are activated during CFC. In addition, TEs were significantly larger on RAM+ compared with RAM− CA3 pyramidal neurons (Figure 6D), suggesting an increase in the number of MF-CA3 synaptic contacts. Taken together, our results provide the first evidence that contextual learning selectively increases MF-CA3 transmission on learning-activated CA3 pyramidal neurons, consistent with the postulated role of MF inputs in encoding contextual memory (Kesner and Rolls, 2015).

Npas4 Deletion Prevents Learning-Induced Modification of MF-CA3 Synapses

We next examined whether the contextual learning-induced changes in MF-CA3 synapses are abolished when Npas4 is acutely deleted in CA3 pyramidal neurons. AAV-Cre-GFP or AAV-ΔCre-GFP was stereotaxically co-injected with AAV-RAM-mKate2 into CA3. Neurons activated by CFC were labeled using a similar procedure as that described above (Figure 6B). In Npas4 cKO mice injected with the control virus AAV-ΔCre-GFP, which does not cause deletion of Npas4, RAM+ neurons showed a significantly higher mEPSC frequency compared with neighboring RAM− neurons, which was abolished by LY354740 treatment, and no difference in mEPSC amplitude (Figure 6E), equivalent to our results in wild-type mice (Figure 6C). However,

(D) Representative experiments of MF-CA3 EPSCs elicited by minimal stimulation in WT and Npas4 KO mice. Shown are superimposed individual traces (top) and time course plots (bottom). Adding DCG-IV (1 μM) at the end of the experiments blocked synaptic transmission (traces not shown).
(E) Summary data showing efficacy: WT, 43.3 ± 8.9 pA; KO, 132.8 ± 25.7 pA; p = 0.0027. Potency: WT, 78 ± 13.4 pA; KO, 184 ± 34.1 pA; p = 0.003. Failure rate: WT, 28.7% ± 4.6%; KO, 30.5% ± 4.8%; p = 0.68. WT: 8 slices, 6 mice; KO: 6 slices, 4 mice.
(F) Short-term plasticity was not altered in Npas4 KO mice. Extracellular MF synaptic responses (fEPSPs) were recorded in acute hippocampal slices from Npas4 KO mice and their WT littermates at 8–10 weeks of age. Sample traces and summary plots are shown. Left: the PPR was assessed by delivering paired pulses at 10-, 30-, 100-, 300-, and 1,000-ms inter-stimulus intervals, and pulse $(P)_2/P_1$ are plotted. Right: frequency facilitation was probed by 5 consecutive pulses at 40-ms intervals, and P_n/P_1 are plotted. WT: n = 7 slices, 3 animals; KO: n = 8 slices, 3 animals.
(G) LTP at MF-CA3 synapses was normal in Npas4 KO mice. LTP was induced with a train of 125 stimuli at 25 Hz. DCG-IV (1 μM) was added at the end of each experiment. Representative traces are shown on the top and summary plots on the bottom. LTP (percent of the baseline for the last 10 min): WT, 152.16% ± 2.52%, n = 7 slices, 3 animals; KO, 152.74% ± 2.01%, n = 8 slices, 3 animals; p = 0.55.
All summary data are shown as mean ± SEM. In (C)–(G), **p < 0.01, Mann-Whitney *U* test. n.s., non-significant. See also Figures S2 and S3.

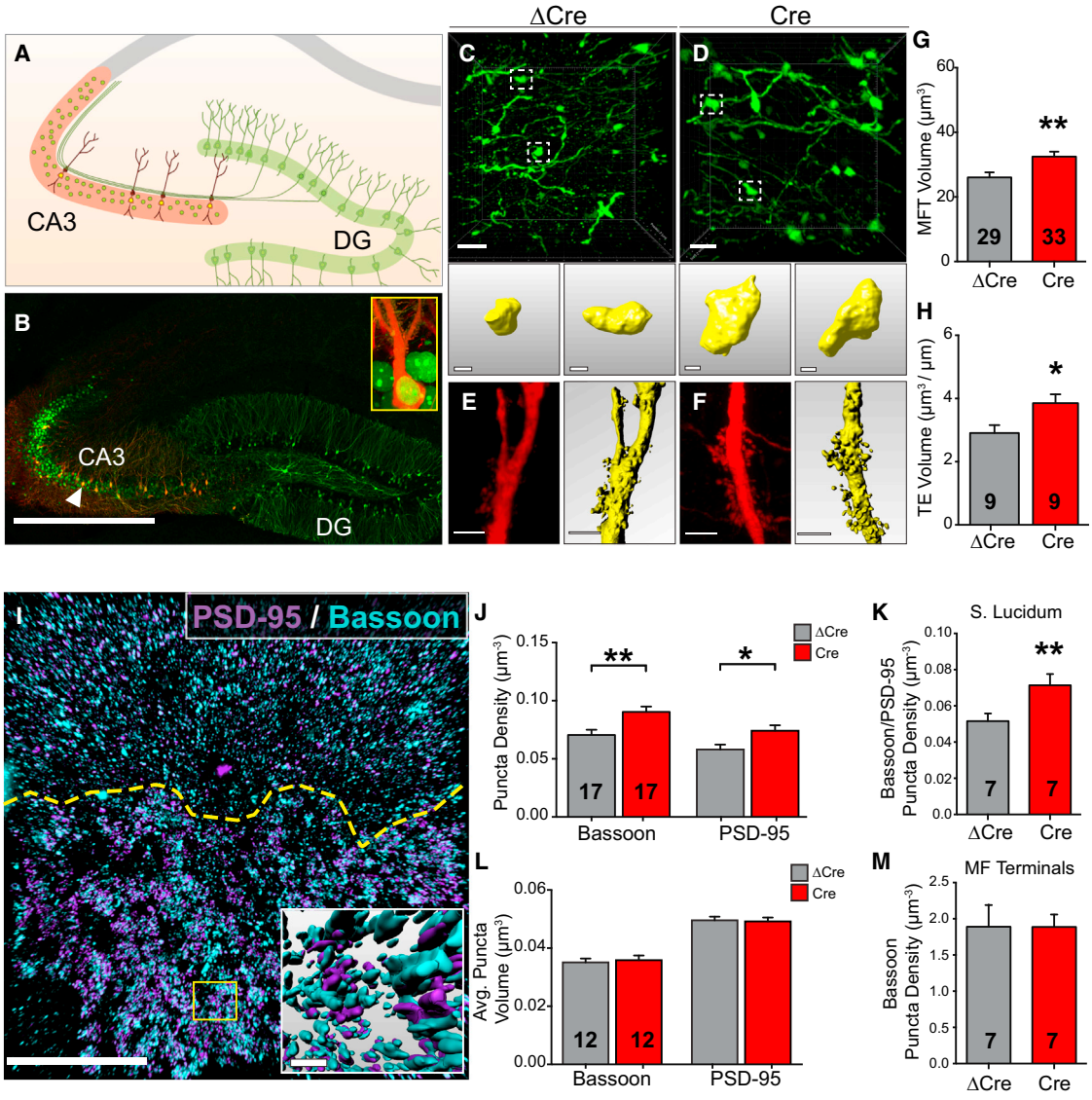

Figure 4. Npas4 Modifies the Number and Structure of MF-CA3 Synapses

(A) Schematic of the labeling strategy with CA3 pyramidal cells expressing nuclearly localized Cre-GFP or ΔCre-GFP and cytosolic tdTomato to label morphology. MF projections from the DG are labeled with both cytosolic and membrane-bound farnesylated GFP.

(B) Representative low-resolution image of two-color labeling of CA3 pyramidal cells (red, tdTomato) and DG cells and their MF projections (green, GFP). Inset: enlarged representation of a CA3 pyramidal cell with nuclear expression of either Cre or ΔCre (green). Scale bar, 500 μm.

(C and D) Top: representative images of MF terminals expressing GFP in the *stratum lucidum* of CA3 under ΔCre (C) or Cre (D) conditions. Bottom: examples of 3D surface reconstruction of large single MF terminals. Scale bars, 10 μm and 1 μm.

(E and F) Representative images of TEs on a proximal CA3 dendrite segment (left) and partial 3D surface reconstruction of a dendritic segment (right) for ΔCre (E) and Cre (F) conditions. Scale bars, 5 μm.

(G) MF terminals that synapse onto Npas4-deleted cells have significantly increased volumes. Volume: ΔCre, 26.06 ± 1.56, n = 29 MF terminals, 3 animals; Cre, 32.48 ± 1.53, n = 33 MF terminals, 3 animals; p = 0.0065.

(H) The volume of TE structures is significantly increased in Npas4-deleted cells. Volume: ΔCre, 2.91 ± 0.25, n = 9, 3 animals; Cre, 3.85 ± 0.28, n = 9, 3 animals; p = 0.04.

(I) Representative image of MAP-processed sections with labeling of the synaptic markers PSD-95 (magenta) and Bassoon (cyan). The inset shows a 3D surface reconstruction of synaptic marker puncta in the region marked with a yellow box. The dashed line indicates the boundary between the *stratum lucidum* and *radiatum* in CA3. Scale bars, 10 μm and 1 μm.

(J) The density of pre- and post-synaptic marker puncta is significantly increased in the *stratum lucidum* of Npas4-deleted cells. Synaptic density: Bassoon, ΔCre 0.07 ± 0.004, n = 17 regions, 6 animals; Bassoon, Cre 0.09 ± 0.004, n = 17 regions, 6 animals; p = 0.008; PSD-95, ΔCre 0.06 ± 0.004, n = 17 regions, 6 animals; PSD-95, Cre 0.07 ± 0.005, n = 17 regions, 6 animals; p = 0.02.

(K) The density of co-localized Bassoon and PSD-95 puncta is significantly increased in the *lucidum* of Npas4-deleted mice. Synaptic density: Bassoon, ΔCre 0.05 ± 0.004, n = 17 regions, 6 animals; Cre 0.07 ± 0.006, n = 17 regions, 6 animals; p = 0.007.

(legend continued on next page)

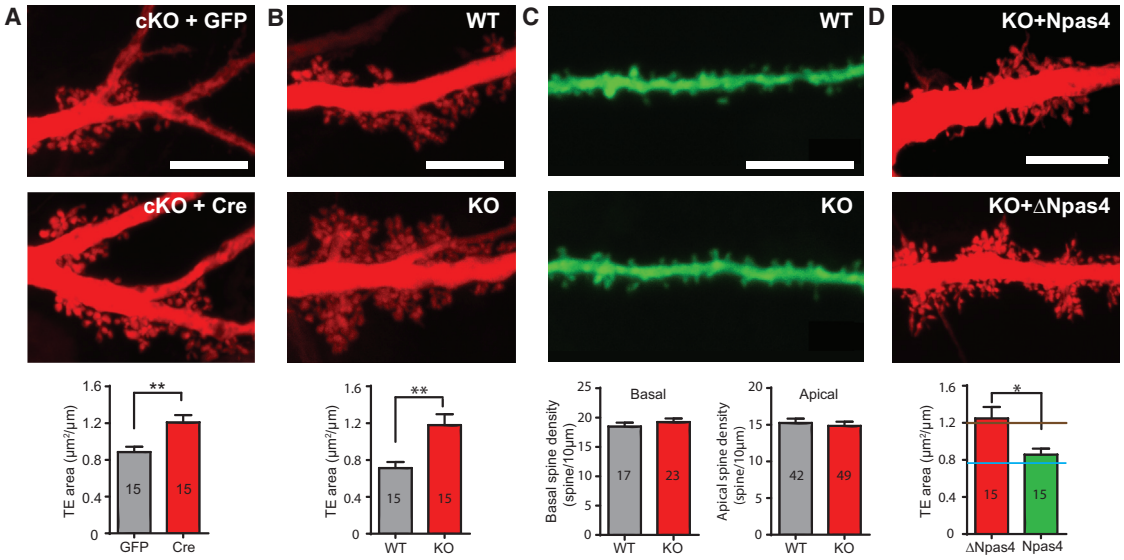

Figure 5. Npas4 Bi-directionally Regulates TE Size

(A) Representative images and summary bar graphs showing that the total area of CA3 TE is significantly increased when Npas4 is deleted by AAV-Cre in Npas4$^{flx/flx}$ mice compared with littermate controls injected with AAV-GFP. TE area: GFP, 0.89 ± 0.06 μm^2/μm, n = 15, 3 animals; Cre, 1.21 ± 0.08 μm^2/μm, n = 15, 3 animals; p = 0.0014.

(B) Representative images and summary bar graphs showing a significantly larger total area of CA3 TE in Npas4 KO mice than in their WT littermates. TE area: WT, 0.71 ± 0.07 μm^2/μm, n = 15 neurons, 3 animals; KO, 1.18 ± 0.12 μm^2/μm, n = 15 neurons, 3 animals; p = 0.0032.

(C) Representative images and summary bar graphs showing comparable spine density on distal dendrites of CA3 pyramidal neurons in Npas4 KO mice and their WT littermates. Number of basal spines per 10 μm: WT, 18.49 ± 0.64; KO, 19.25 ± 0.59; p = 0.43. Number of apical spines per 10 μm: WT, 15.25 ± 0.58; KO, 14.84 ± 0.57; p = 0.64. WT basal: n = 17 dendrites, 2 animals; KO basal: n = 23 dendrites, 3 animals; WT apical: n = 42 dendrites, 7 animals; KO apical: n = 49 dendrites, 8 animals.

(D) Representative images and summary bar graphs showing that Npas4 expression in Npas4 KO mice reduced CA3 TE size to the WT level. TE area: ΔNpas4, 1.25 ± 0.12 μm^2/μm; Npas4, 0.86 ± 0.06 μm^2/μm; n = 15 neurons, 3 animals for each condition; p = 0.013. The blue and brown lines indicate the TE area values of Npas4 WT and KO mice, respectively.

Scale bars correspond to 5 μm. Summary data are shown as mean ± SEM. *p < 0.05, **p < 0.01, Mann-Whitney *U* test.

after deletion of Npas4, there was no difference in either mEPSC frequency or amplitude between RAM+ and RAM− neurons, presumably because of the robust elevation of mEPSC frequency in both RAM+ and RAM– neurons that results from Npas4 deletion (Figure 6F). These data suggest that Npas4 deletion prevents the learning-induced modification of MF-CA3 synapses that may be responsible for the impairment in contextual memory formation we observed upon Npas4 deletion.

So far, our results suggest that Npas4 selectively restricts the number of functional synaptic contact established by an MF terminal onto a CA3 pyramidal neuron. Because Npas4 expression is selectively regulated by neuronal activity (Lin et al., 2008; Ramamoorthi et al., 2011), and MF-CA3 synapses are very sensitive to changes in the levels of neuronal activity (Kim and Tsien, 2008; Lee et al., 2013), we wondered whether Npas4 is involved in homeostatic shrinkage of TEs in response to neuronal activity within CA3. To address this question, we artificially increased the activity level in CA3 pyramidal neurons by expressing the bacterial sodium channel NaChBac, which renders neurons hyperexcitable (Ren et al., 2001) and has been used to induce homeostatic changes in neurons (Sim et al., 2013; Xue et al., 2014). AAV-CaMKII-NaChBac-mCherry or control AAV-CaMKII-NaChBac^{mut}-mCherry expressing the non-conducting mutant form NaChBac^{mut} (Yue et al., 2002) was stereotaxically injected into Npas4 cKO mice together with either AAV-Cre-GFP or AAV-ΔCre-GFP (to express GFP in the nucleus). To visualize TE morphology in a sparse population of neurons, we co-injected diluted AAV-EF1α-Flp^o and AAV-hSyn-fDIO-GFP-P2A-^{farn}GFP (Figures 7A and 7B). Ten days after viral injection, neurons expressing NaChBac displayed prolonged action potentials and hyperexcitability, as reported previously (Ren et al., 2001; Sim et al., 2013; Xue et al., 2014), compared with those expressing NaChBac^{mut}, which have similar properties as uninfected neurons (Figure 7C). As expected, deletion of Npas4 significantly

(L) The average synaptic punctum volume does not change when Npas4 is deleted. Average volume: Bassoon, ΔCre 0.05 ± 0.004, n = 12 regions, 6 animals; Cre 0.05 ± 0.001, n = 12 regions, 6 animals; p = 0.57; PSD-95, ΔCre 0.04 ± 0.003, n = 12 regions, 6 animals; PSD-95, Cre 0.04 ± 0.002, n = 12 regions, 6 animals; p = 0.42.

(M) The density of Bassoon puncta localized within MF terminals does not change in Npas4-deleted cells. Synaptic density: Bassoon, ΔCre 1.89 ± 0.31, n = 12 regions, 6 animals; Cre 1.89 ± 0.17, n = 12 regions, 6 animals; p = 0.98.

Summary data are shown as mean ± SEM. *p < 0.05, **p < 0.01, Mann-Whitney *U* test.

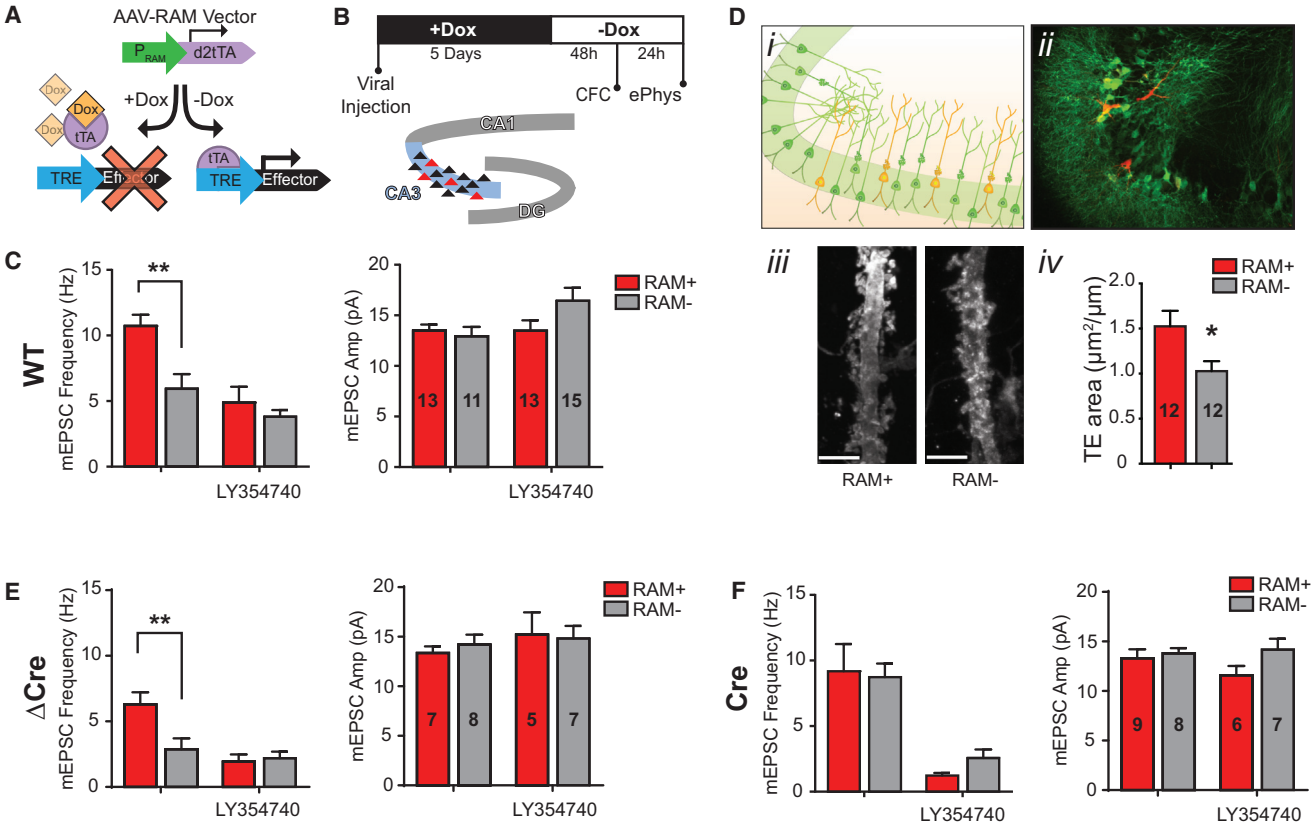

Figure 6. Contextual Learning Selectively Strengthens MF Inputs, and Npas4 Deletion Prevents This Experience-Dependent Modulation

(A) The design of the RAM system. The RAM promoter P_{RAM} drives the expression of a destabilized version of the tetracycline transactivator (d2tTA), which subsequently drives the expression of the reporter gene under the control of a tTA-responsive element (TRE) in the promoter. The binding of d2tTA to TRE and, as a result, the expression of the reporter gene can be blocked by the antibiotic doxycycline (Dox).

(B) Experimental timeline. Animals were taken off the Dox diet 5 days after virus injection and 48 hr before CFC training and sacrificed 24 hr later for electrophysiological recordings.

(C) WT C57BL/6 mice were co-injected with AAV-RAM-mKate2 and AAV-EF1α-GFP (as an infection control). RAM+ CA3 pyramidal neurons have a significantly higher mEPSC frequency than their neighboring RAM− neurons, whereas LY354740 (300 nM) abolishes this difference. Frequency: control RAM+, 10.72 ± 0.86 Hz; control RAM−, 5.93 ± 1.13 Hz; LY354740 (LY) RAM+, 4.88 ± 1.21 Hz; LY RAM−, 3.81 ± 0.5 Hz; F (1, 48) = 3.975, p = 0.05. Amplitude: control RAM+, 13.47 ± 0.6 pA; control RAM−, 12.92 ± 0.92 pA; LY RAM+, 13.45 ± 1.05 pA; LY RAM−, 16.42 ± 1.3 pA; F (1, 48) = 2.829, p = 0.1. Control RAM+: n = 13, control RAM−: n = 11, LY RAM+: n = 13, LY RAM−: n = 15; 6 animals.

(D) 2D morphological analysis of RAM+ and RAM− neurons. (i) Schematic showing the sparse labeling strategy in CA3 pyramidal cells with RAM+ cells labeled in orange (GFP and tdTomato) and RAM− cells labeled in green (GFP only). (ii) Representative image of CA3 following the labeling scheme in (i). (iii) Representative images of dendritic segments with TEs of RAM+ and RAM− cells. (iv) 2D quantification of TE areas. TE area: RAM+, 1.52 ± 0.17, n = 12 dendrites, 5 animals; RAM−, 1.03 ± 0.11, n = 12 dendrites, 5 animals; p = 0.0296.

(E) Npas4 cKO mice were co-injected with AAV-RAM-mKate2 and AAV-hSyn-ΔCre-GFP. RAM+ CA3 pyramidal neurons have a significantly higher mEPSC frequency than their neighboring RAM− neurons, whereas LY354740 (300 nM) abolishes this difference. Frequency: control RAM+, 6.31 ± 0.91 Hz; control RAM−, 2.88 ± 0.82 Hz; LY RAM+, 1.95 ± 0.54 Hz; LY RAM−, 2.19 ± 0.51; F (1, 23) = 5.653, p = 0.026. Amplitude: control RAM+, 13.36 ± 0.67 pA; control RAM−, 14.2 ± 1.01 pA; LY RAM+, 15.21 ± 2.25 pA; LY RAM-, 14.82 ± 1.28 pA; F (1, 23) = 0.2331, p = 0.63. Control RAM+: n = 7, control RAM−: n = 8, LY RAM+: n = 5, LY RAM−: n = 7; 5 animals.

(F) Npas4 cKO mice were co-injected with AAV-RAM-mKate2 and AAV-hSyn-Cre-GFP. The mEPSC frequency for both RAM+ and RAM− was elevated by Npas4 deletion, but the difference between them was abolished. Frequency: control RAM+, 9.19 ± 2.08 Hz; control RAM−, 8.73 ± 1.03 Hz; LY RAM+, 1.24 ± 0.19 Hz; LY RAM−, 2.57 ± 0.65 Hz; F (1, 26) = 0.3899, p = 0.54. Amplitude: control RAM+, 13.31 ± 0.9 pA; control RAM−, 13.81 ± 0.52 pA; LY RAM+, 11.58 ± 0.94 pA; LY RAM−, 14.17 ± 1.1; F (1, 26) = 1.39, p = 0.25. Control RAM+: n = 9, control RAM−: n = 8, LY RAM+: n = 6, LY RAM−: n = 7; 3 animals.

Summary data are shown as mean ± SEM. In (C), (E), and (F), **p < 0.01, two-way ANOVA, Bonferroni's post hoc test. In (D), *p < 0.05, Mann-Whitney *U* test. See also Figure S4.

increased TE size (Figure 7E, compare the Cre and ΔCre conditions with expression of $NaChBac^{Mut}$). Interestingly, NaChBac expression caused a significant homeostatic reduction in TE size both with and without Npas4 (Figure 7E). This observation suggests that Npas4 is not generally required for activity-dependent homeostatic reduction of MF-CA3 synapses but also that the impaired contextual memory formation in the absence of Npas4 is likely due to loss of the specific learning-induced

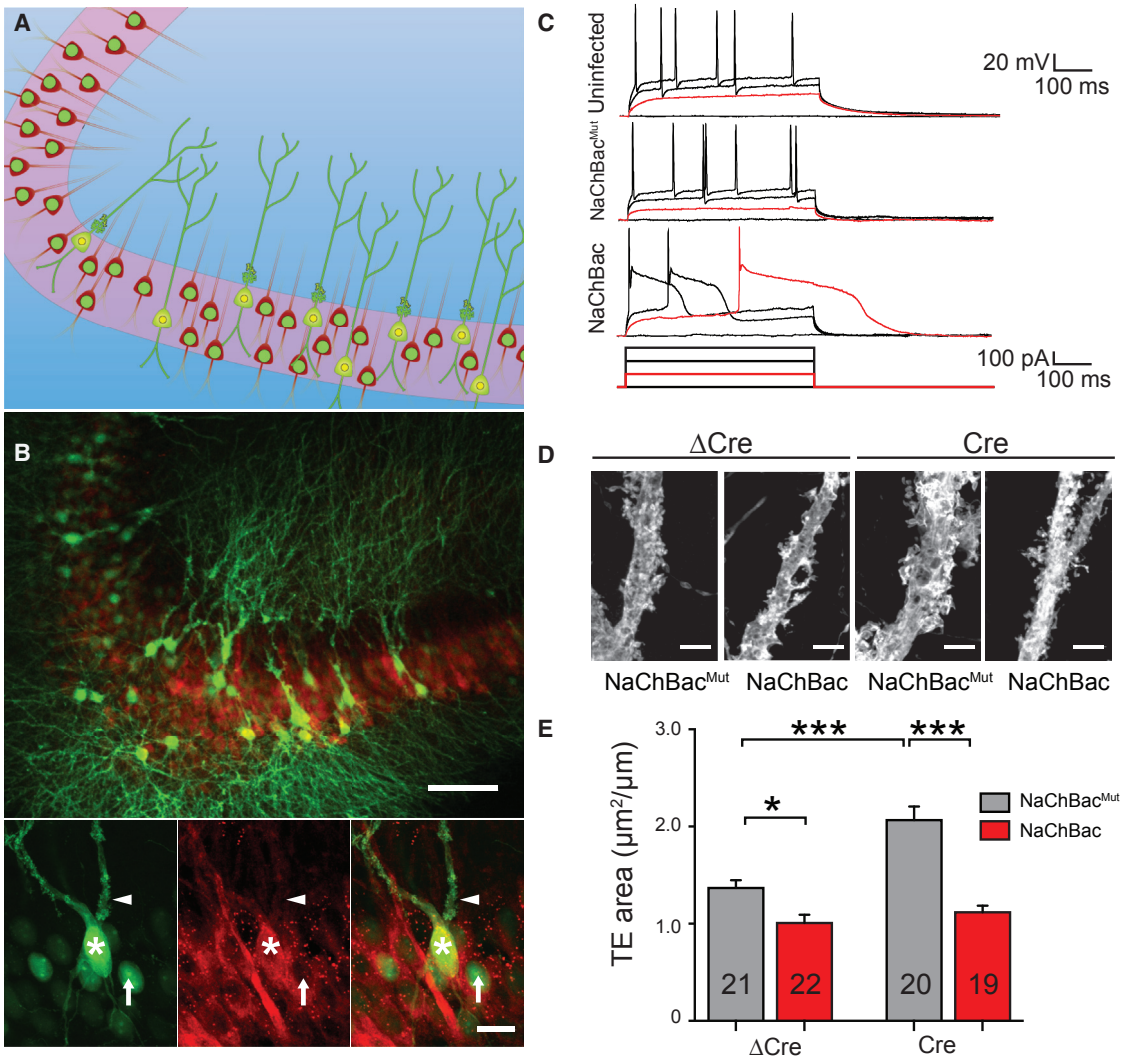

Figure 7. Npas4 Is Not Required for Activity-Dependent Homeostatic Shrinkage of TE Structures

(A) Schematic showing the sparse labeling strategy in CA3 pyramidal cells with morphology in green (GFP) and NaChBac or NaChBac^{mut} cells labeled in red (tdTomato). CA3 pyramidal cells also expressed nuclearly localized Cre-GFP or ΔCre-GFP as a control.

(B) Representative image of CA3 cells following the labeling scheme in (A). Bottom: high-magnification image of a cell expressing cytosolic GFP to label morphology (arrowhead) and nuclear Cre-GFP (*); neighboring cells expressed only nuclear Cre-GFP (arrow). Cells also expressed mCherry in the presence of NaChBac or NaChBach^{Mut}. Scale bars, = 100 and 10 μm, respectively.

(C) Representative traces from electrophysiological recordings of uninfected cells and cells expressing NaChBac or NaChBac^{Mut} 10 days after virus injection.

(D) Representative images of dendritic segments with TE structures. Scale bars, 5 μm.

(E) 2D quantification of TE areas. TE area: ΔCre + NaChBac, 1.01 ± 0.09 μm^2/μm, n = 21 cells; ΔCre + NaChBac^{Mut}, 1.37 ± 0.08 μm^2/μm, n = 22 cells; Cre + NaChBac, 1.12 ± 0.07 μm^2/μm, n = 20 cells; Cre + NaChBac^{Mut}, 2.07 ± 0.14, n = 19 cells. 3 mice per condition, $F(1,78) = 9.343$, $p = 0.0031$. *$p < 0.05$, **$p < 0.01$, ***$p < 0.001$. Two-way ANOVA with Tukey's *post hoc* multiple comparisons test. Summary data are shown as mean ± SEM.

modulation of MF-CA3 synapses rather than a general disruption of homeostatic balance in CA3.

Npas4 Regulates MF-CA3 Synapses via Its Transcriptional Target Plk2

Npas4 is a transcription factor and exerts its effects on neural circuits by regulating the expression of downstream transcriptional targets. One such target, brain-derived neurotrophic factor (BDNF), has been shown to mediate the effect of Npas4 on GABAergic inhibitory synapses in CA1 (Bloodgood et al., 2013; Lin et al., 2008; Ramamoorthi et al., 2011). To determine whether BDNF is also involved in the regulation of MF-CA3 synapses by Npas4, we removed the BDNF gene from CA3 pyramidal neurons of BDNF cKO (BDNF$^{flx/flx}$) mice (Rios et al., 2001) by stereotaxic injection of AAV-Cre. This manipulation caused a significant reduction in mIPSC amplitude in CA3 pyramidal neurons, indicating effective deletion of BDNF. However, deletion of BDNF in CA3 had no effect on mEPSCs, suggesting that a

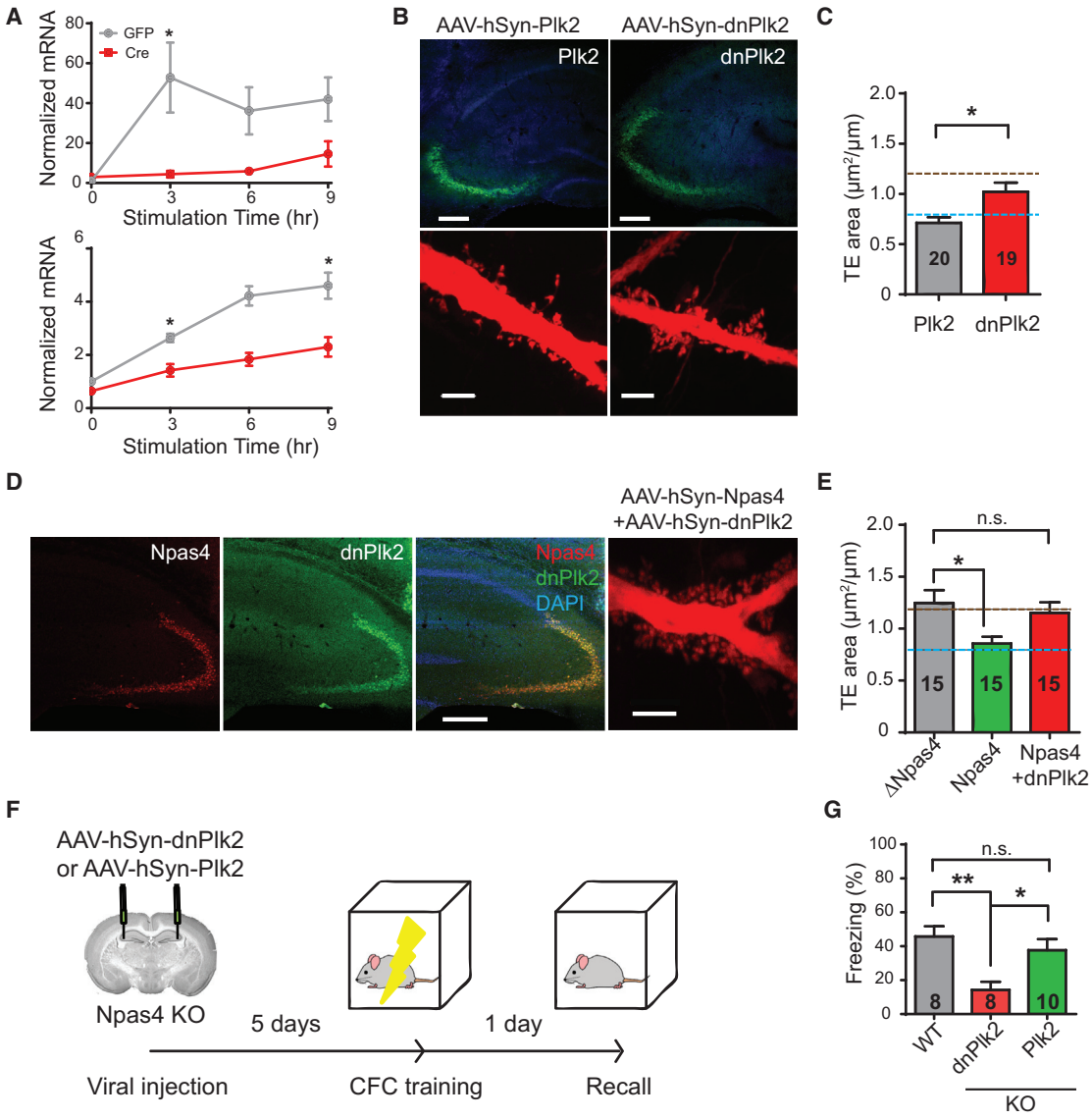

Figure 8. Npas4 Mediates Activity-Dependent Modulation of TEs through Its Transcriptional Target Plk2

(A) Npas4 controls the activity-dependent expression of Plk2. Cultured hippocampal neurons from Npas4$^{flx/flx}$ mice were infected with AAV1-hSyn-GFP-Cre (Cre) or AAV1-hSyn-GFP (GFP) virus on day in vitro 9 (DIV9) and then stimulated with 10 μM kainic acid on DIV15 for 3, 6, and 9 hr before being lysed for RT-PCR analysis. 0 hr represents the unstimulated conditions. mRNA levels were normalized to Tuj1 expression levels. Data were derived from 4 independent experiments. *p < 0.05, Mann-Whitney *U* test.

(B and C) Selective expression of Plk2 in CA3 reduces TE size in Npas4 KO mice, whereas expression of the dominant-negative form of Plk2 (dnPlk2) fails to increase TE size further. AAV-hSyn-Plk2-FLAG or AAV-hSyn-dnPlk2-FLAG were stereotaxically injected into the hippocampus of Npas4 KO mice.

(B) Representative images showing Plk2 and dnPlk2 overexpression and the corresponding TEs in CA3 of Npas4 KO mice. Scale bars correspond to 200 μm on the top and 5 μm on the bottom.

(C) Summary bar graphs of TE size analysis in Npas4 KO mice injected with AAV-hSyn-Plk2-FLAG or AAV-hSyn-dnPlk2-FLAG. TE area: Plk2, 0.71 ± 0.05 μm^2/μm; dnPlk2, 0.99 ± 0.09 μm^2/μm; p = 0.026; n = 20 and 19 neurons, respectively, 4 animals for each condition. *p < 0.05, Mann-Whitney *U* test.

(D and E) The effect of Npas4 expression in CA3 of Npas4 KO, which previously reduced the TE size to the WT level, was blocked by dnPlk2. Npas4 KO mice were stereotaxically injected with AAV-hSyn-ΔNpas4-HA, AAV-hSyn-Npas4-HA, or AAV-hSyn-Npas4-HA and AAV-hSyn-dnPlk2-FLAG.

(D) Representative images showing Npas4 (red) and Plk2 (green) expression in CA3 of Npas4 KO mice co-injected with AAV-hSyn-Npas4-HA and AAV-hSyn-dnPlk2-FLAG. The scale bar corresponds to 300 μm. A representative image of TEs is shown on the right, and the scale bar there corresponds to 5 μm.

(E) Summary bar graph of TE size in Npas4 KO mice infected with AAV-hSyn-ΔNpas4-HA or AAV-hSyn-Npas4-HA or co-infected with AAV-hSyn-Npas4-HA and AAV-hSyn-dnPlk2-FLAG. TE area: ΔNpas4, 1.25 ± 0.12 μm^2/μm; Npas4, 0.86 ± 0.06 μm^2/μm; Npas4 + dnPlk2, 1.15 ± 0.10 μm^2/μm; F (2, 42) = 4.396; p = 0.019; n = 15 neurons, 3 animals per condition. *p < 0.05, one-way ANOVA, Dunnett's *post hoc* test. The data for Npas4 and ΔNpas4 conditions are re-plotted from Figure 5D.

(F and G) Resetting TE size in Npas4 KO mice rescues the contextual memory deficit.

(legend continued on next page)

different transcriptional target of Npas4 mediates its effect on MF-CA3 synapses (Figure S5).

The activity-regulated gene Plk2 has been implicated in activity-dependent shrinkage of dendritic spines (Evers et al., 2010; Lee et al., 2011; Pak and Sheng, 2003; Seeburg et al., 2008), and a dominant-negative form of Plk2 (dnPlk2) has been reported to enlarge TEs (Lee et al., 2013). Npas4 chromatin immunoprecipitation sequencing (ChIP-seq) data (Kim et al., 2010) indicate that Npas4 binds to the promoter and enhancers of Plk2, suggesting that Plk2 is a direct transcriptional target of Npas4 (Figure S6). Consistent with this idea, Npas4 deletion from hippocampal neurons prepared from Npas4 cKO mice significantly reduced the activity-dependent expression of Plk2 (Figure 8A).

We then designed epistasis experiments to test the hypothesis that Plk2 acts downstream of Npas4 to modulate TE size in MF-CA3 synapses. If this hypothesis is true, then abolishing the activity of both Npas4 and Plk2 should not have an additive effect; therefore, blocking Plk2 function in Npas4 KO mice by expressing dnPlk2 should not cause any further increase in TE size. To test this, AAVs expressing dnPlk2 or wild-type Plk2 were stereotaxically delivered to CA3 of Npas4 KO mice, and TE areas were measured 3 days later (Figure 8B). Overexpression of dnPlk2 did not cause any additional enlargement of TEs, consistent with Plk2 functioning downstream of Npas4 (Figure 8C). Overexpression of wild-type Plk2, which bypasses the requirement for Npas4, significantly reduced the TE area (Figure 8C). If Plk2 mediates the effect of Npas4 on TE size, then dnPlk2 should block this effect. Re-expressing Npas4 in CA3 of Npas4 KO mice not only rescues the contextual learning deficit (Ramamoorthi et al., 2011) but also restores changes in mEPSCs (Figures 2E–2G) and reduces the TE size to wild-type levels (Figure 5D). However, co-expression of dnPlk2 completely prevented Npas4 from restoring TE sizes to normal (Figure 8E). We conclude that Npas4 likely exerts its effect on MF-CA3 TEs by activating Plk2 expression.

Our findings suggest that contextual memory formation depends on Npas4 restricting the number of MF-CA3 synaptic contacts. If this is true, then resetting MF-CA3 synapses to the wild-type level by expressing the Npas4 downstream target Plk2 should restore contextual memory formation. Indeed, we found that Plk2 overexpression in CA3 of Npas4 KO mice (Figure 8F) restored TEs to a size comparable with wild-type littermates (Figure 8C). Some mice in each behavioral cohort were injected with dnPlk2 as controls. Remarkably, although overexpression of either Plk2 or dnPlk2 did not affect the behavior of wild-type mice (Figure S7), Npas4 KO mice overexpressing wild-type Plk2 were able to form contextual memories, exhibiting similar freezing behavior as their wild-type littermates (Figure 8G). Npas4 KO mice overexpressing dnPlk2 remained defective in forming contextual memories (Figure 8G). These results indicate that restriction of the number of MF-CA3 synaptic contacts by Npas4 is critical for the encoding of new contextual information.

DISCUSSION

Here we provide evidence for a molecular pathway that selectively regulates the critical excitatory MF input into CA3 for encoding contextual memory. To the best of our knowledge, Npas4, which we previously showed to be required in CA3 for contextual memory formation (Ramamoorthi et al., 2011), emerges as the first gene with such a specific role in CA3-dependent contextual memory formation. In addition, our study also uncovers a form of learning-induced plasticity that occurs specifically at the MF-CA3 synapses. Furthermore, this experience-dependent synaptic plasticity at MF-CA3 synapses is under the control of Npas4. Last, we have identified Plk2 as the downstream transcriptional target of Npas4 that mediates its effect on MF-CA3 synapses. Altogether, our findings reveal a novel molecular and synaptic mechanism underlying long-term contextual memory formation in CA3. Our results suggest a molecular cascade in which Npas4 is activated by neuronal activity and induces the expression of Plk2, which, in turn, restricts the number of functional contacts between MF terminals and CA3 pyramidal neurons. Notably, Npas4 selectively regulates MF inputs but not other excitatory (or inhibitory) synaptic inputs converging on CA3 pyramidal neurons. Considering that Npas4 is selectively induced by neuronal activity (Lin et al., 2008; Ramamoorthi et al., 2011), its selective regulation of MF-CA3 synapses might be determined by the unique features of MF transmission, including robust frequency facilitation and strong postsynaptic drive, which are distinct from those received from the perforant and recurrent paths (Henze et al., 2000, 2002; Urban et al., 2001). In other words, Npas4 may be preferentially induced by activity input from MF pathways. This could explain why, although it appears to homeostatically regulate MF-CA3 synapses, Npas4 is not required for homeostatic change at those synapses in response to a global, non-MF-specific activity increase caused by NaChBac expression (Figure 7).

Npas4 has previously been shown to engage different downstream transcriptional targets in different cell types and brain regions to modify synaptic connections (Bloodgood et al., 2013; Lin et al., 2008; Sim et al., 2013; Spiegel et al., 2014; Yoshihara et al., 2014). Most notably, BDNF mediates the effects of Npas4 in recruiting GABAergic inhibitory synapses onto CA1 pyramidal neurons in response to activity (Bloodgood et al., 2013; Lin et al., 2008). Intriguingly, Npas4 does not appear to modulate GABAergic synapses on CA3 pyramidal neurons, at

(F) Npas4 KO mice were stereotaxically injected with AAV1-hSyn-dnPlk2 or AAV1-hSyn-Plk2 in CA3. Five days after surgery, mice underwent CFC, and their contextual memories were tested 24 hr later.

(G) Summary bar graph showing that Npas4 KO mice injected with Plk2 displayed similar freezing levels as their WT littermates, whereas those injected with dnPlk2 continued to display impaired contextual memory. Freezing level: WT, 45.83% ± 6.85%; KO + dnPlk2, 14.32% ± 5.44%; KO + Plk2, 37.71% ± 7.24%; $F(2, 23) = 7.135$; $p = 0.0039$. *$p < 0.05$, **$p < 0.01$, one-way ANOVA, Tukey's *post hoc* test.

The blue and brown horizontal lines in (C) and (E) indicate the TE areas seen in Npas4 WT and KO mice, respectively (Figure 5C). All summary data are shown as mean ± SEM. See also Figures S5–S7.

least under the conditions we have tested. We currently do not know what additional cellular mechanisms determine the varying effects of Npas4 in different cell types and brain regions.

Our study also uncovered a form of learning-induced structural and functional plasticity that occurs specifically at the MF-CA3 synapses during contextual memory formation. We have shown that contextual learning selectively strengthens MF inputs onto the group of CA3 pyramidal neurons that is activated during learning. These so-called ensemble neurons have been shown to be involved in memory encoding (Denny et al., 2014; Liu et al., 2012), but synaptic plasticity on these neurons specifically induced by learning has not been widely explored. Although previous studies have provided an abundance of evidence that MF-CA3 synapses are modified by experience (Galimberti et al., 2006; Gogolla et al., 2009; Magariños et al., 1997; Maruo et al., 2016; Rekart et al., 2007; Sandi et al., 2003), they have typically relied on chronic behavioral manipulations to induce changes in MF-CA3 synapses. Consequently, it is difficult to determine whether these changes are the result of specific learning experience or a consequence of network-wide homeostatic adaptation, especially because MF-CA3 synapses are highly sensitive to homeostatic changes (Chater and Goda, 2013; Kim and Tsien, 2008; Lee et al., 2013). To the best of our knowledge, we are the first to demonstrate a synaptic change on CA3 ensemble neurons that is specifically induced by contextual learning.

MF inputs to CA3 pyramidal neurons are required for contextual memory encoding (Jerman et al., 2006; Lassalle et al., 2000; Lee and Kesner, 2004a) and the learning-induced functional and structural change we describe here appears to selectively occur at MF-CA3 synapses. The fact that Npas4 deletion prevents MF-CA3 synaptic modulation and also impairs contextual memory formation suggests that the learning-induced synaptic modulation we found plays an important role in contextual memory formation. Npas4 deletion in CA3 strongly increases the number of synaptic contacts established by a single MF terminal onto a CA3 pyramidal neuron. In the absence of Npas4, strengthened MF inputs could reach the ceiling of their dynamic range and no longer be modified by learning, disrupting the formation of a sparse engram. Thus, Npas4 could be required for maintaining MF inputs within their normal dynamic range. Although we identify Npas4 as a critical regulator of the experience-dependent plasticity at MF-CA3 synapses, the molecular pathways responsible for the selective strengthening of the MF input caused by learning are currently unknown.

Enhanced connectivity between DG granule cells to CA3 pyramidal neurons has long been postulated to be a key feature of the computational mechanism by which CA3 encodes new contextual representations transmitted from the DG (Cerasti and Treves, 2010; Treves and Rolls, 1992). The robust increase in the number of MF-CA3 synaptic contacts induced by Npas4 deletion could also include enhanced DG-CA3 connectivity, a possibility we cannot completely rule out. It is intriguing that Npas4 regulates the number of MF-CA3 functional contacts but not their dynamic properties (i.e., short-term and long-term plasticity). Contextual learning itself also increases the number of functional MF-CA3 synaptic contacts on CA3 pyramidal neurons activated by learning. The computational benefit of modulating MF-CA3 synapse number selectively is currently unknown and warrants future investigation.

STAR★METHODS

Detailed methods are provided in the online version of this paper and include the following:

- KEY RESOURCES TABLE
- CONTACT FOR REAGENT AND RESOURCE SHARING
- EXPERIMENTAL MODEL AND SUBJECT DETAILS
- METHOD DETAILS
  - Acute Slice Preparation
  - Viral Vectors
  - Stereotaxic Injection
  - Sparse Cell Labeling Strategy
  - Seizure Induction and *In Vivo* Activity Manipulation
  - Immunohistochemistry
  - Stick and Stain
  - SeeDB2
  - MAP
  - 2D Spine Density and TE Morphology
  - 3D Reconstruction of MF, TE, and Synaptic Puncta
  - Contextual Fear Conditioning
  - Neuronal Cultures and qRT-PCR
  - RT-PCR Analysis
- QUANTIFICATION AND STATISTICAL ANALYSIS

SUPPLEMENTAL INFORMATION

Supplemental Information includes seven figures and can be found with this article online at https://doi.org/10.1016/j.neuron.2018.01.026.

ACKNOWLEDGMENTS

We thank C. Mark Fletcher and Charles Jennings for critical reading of the manuscript; Matthew Wilson, Howard Eichenbaum, and members of the Lin lab for discussions and comments regarding the study; Qiang Chang for kindly providing the BDNF$^{flx/flx}$ mice; Mollie Meffert for kindly providing the Plk2 and dnPlk2 constructs; and Rachel Schecter for help with the stick and stain technique. We are grateful to Li-Huei Tsai and the Picower Institute for Learning and Memory for sharing their microscopy resources. This work was funded by a Swedish Brain Foundation research fellowship (to A.T.S.), Swiss National Science Foundation SNF171978 (to K.Z.), Burroughs Wellcome Fund Career Awards at the Scientific Interface, the Searle Scholars Program, Packard award in Science and Engineering, NARSAD Young Investigator Award, the JBP Foundation, NCSOFT Cultural Foundation, and NIH grant NS090473 (to K.C.), the JPB Foundation (to W.X.), NIH grants DA017392 and MH081935 (to P.E.C.), and the James H. Ferry Fund and NIH grants MH091220, NS088421, and DC014701 (to Y.L.).

AUTHOR CONTRIBUTIONS

F.-J.W. designed and conducted most of the electrophysiology, morphology, and behavior experiments. R.I.G. carried out all 3D morphological reconstruction and high-resolution imaging of MAP-processed samples as well as some other imaging analysis. Y.Z. and D.R. contributed to the morphology and behavior experiments. M.D. conducted the RT-PCR experiments. D.G.-D. and M.H. contributed to spine density measurement. T.D.Y. and A.T.S. assisted with the electrophysiology and behavior experiments. T.K. and K.C. processed samples using MAP for high-resolution synaptic analysis. K.Z. and W.X. carried out sample processing and imaging using the SeeDB2 procedure. S.L., K.A., and P.E.C. assessed the function of evoked MF transmission and

plasticity. Y.L. designed and supervised the study. Y.L. and F.-J.W. wrote the paper with input from all authors.

DECLARATION OF INTERESTS

The authors declare no competing interests.

Received: March 10, 2017
Revised: November 26, 2017
Accepted: January 11, 2018
Published: February 8, 2018

REFERENCES

Alvarez, V.A., and Sabatini, B.L. (2007). Anatomical and physiological plasticity of dendritic spines. Annu. Rev. Neurosci. *30*, 79–97.

Amaral, D.G., and Dent, J.A. (1981). Development of the mossy fibers of the dentate gyrus: I. A light and electron microscopic study of the mossy fibers and their expansions. J. Comp. Neurol. *195*, 51–86.

Ben-Ari, Y., and Represa, A. (1990). Brief seizure episodes induce long-term potentiation and mossy fibre sprouting in the hippocampus. Trends Neurosci. *13*, 312–318.

Bloodgood, B.L., Sharma, N., Browne, H.A., Trepman, A.Z., and Greenberg, M.E. (2013). The activity-dependent transcription factor NPAS4 regulates domain-specific inhibition. Nature *503*, 121–125.

Cerasti, E., and Treves, A. (2010). How informative are spatial CA3 representations established by the dentate gyrus? PLoS Comput. Biol. *6*, e1000759.

Chater, T.E., and Goda, Y. (2013). CA3 mossy fiber connections: giant synapses that gain control. Neuron *77*, 4–6.

Chicurel, M.E., and Harris, K.M. (1992). Three-dimensional analysis of the structure and composition of CA3 branched dendritic spines and their synaptic relationships with mossy fiber boutons in the rat hippocampus. J. Comp. Neurol. *325*, 169–182.

Chierzi, S., Stachniak, T.J., Trudel, E., Bourque, C.W., and Murai, K.K. (2012). Activity maintains structural plasticity of mossy fiber terminals in the hippocampus. Mol. Cell. Neurosci. *50*, 260–271.

Claiborne, B.J., Xiang, Z., and Brown, T.H. (1993). Hippocampal circuitry complicates analysis of long-term potentiation in mossy fiber synapses. Hippocampus *3*, 115–121.

Denny, C.A., Kheirbek, M.A., Alba, E.L., Tanaka, K.F., Brachman, R.A., Laughman, K.B., Tomm, N.K., Turi, G.F., Losonczy, A., and Hen, R. (2014). Hippocampal memory traces are differentially modulated by experience, time, and adult neurogenesis. Neuron *83*, 189–201.

Evers, D.M., Matta, J.A., Hoe, H.S., Zarkowsky, D., Lee, S.H., Isaac, J.T., and Pak, D.T. (2010). Plk2 attachment to NSF induces homeostatic removal of GluA2 during chronic overexcitation. Nat. Neurosci. *13*, 1199–1207.

Galimberti, I., Gogolla, N., Alberi, S., Santos, A.F., Muller, D., and Caroni, P. (2006). Long-term rearrangements of hippocampal mossy fiber terminal connectivity in the adult regulated by experience. Neuron *50*, 749–763.

Gogolla, N., Galimberti, I., Deguchi, Y., and Caroni, P. (2009). Wnt signaling mediates experience-related regulation of synapse numbers and mossy fiber connectivities in the adult hippocampus. Neuron *62*, 510–525.

Henze, D.A., Urban, N.N., and Barrionuevo, G. (2000). The multifarious hippocampal mossy fiber pathway: a review. Neuroscience *98*, 407–427.

Henze, D.A., Wittner, L., and Buzsáki, G. (2002). Single granule cells reliably discharge targets in the hippocampal CA3 network in vivo. Nat. Neurosci. *5*, 790–795.

Hofmann, M.E., Nahir, B., and Frazier, C.J. (2008). Excitatory afferents to CA3 pyramidal cells display differential sensitivity to CB1 dependent inhibition of synaptic transmission. Neuropharmacology *55*, 1140–1146.

Jerman, T., Kesner, R.P., and Hunsaker, M.R. (2006). Disconnection analysis of CA3 and DG in mediating encoding but not retrieval in a spatial maze learning task. Learn. Mem. *13*, 458–464.

Jonas, P., Major, G., and Sakmann, B. (1993). Quantal components of unitary EPSCs at the mossy fibre synapse on CA3 pyramidal cells of rat hippocampus. J. Physiol. *472*, 615–663.

Kamiya, H., and Ozawa, S. (1999). Dual mechanism for presynaptic modulation by axonal metabotropic glutamate receptor at the mouse mossy fibre-CA3 synapse. J. Physiol. *518*, 497–506.

Kamiya, H., Shinozaki, H., and Yamamoto, C. (1996). Activation of metabotropic glutamate receptor type 2/3 suppresses transmission at rat hippocampal mossy fibre synapses. J. Physiol. *493*, 447–455.

Ke, M.T., Nakai, Y., Fujimoto, S., Takayama, R., Yoshida, S., Kitajima, T.S., Sato, M., and Imai, T. (2016). Super-resolution mapping of neuronal circuitry with an index-optimized clearing agent. Cell Rep. *14*, 2718–2732.

Kesner, R.P. (2007). Behavioral functions of the CA3 subregion of the hippocampus. Learn. Mem. *14*, 771–781.

Kesner, R.P., and Rolls, E.T. (2015). A computational theory of hippocampal function, and tests of the theory: new developments. Neurosci. Biobehav. Rev. *48*, 92–147.

Kim, J., and Tsien, R.W. (2008). Synapse-specific adaptations to inactivity in hippocampal circuits achieve homeostatic gain control while dampening network reverberation. Neuron *58*, 925–937.

Kim, T.K., Hemberg, M., Gray, J.M., Costa, A.M., Bear, D.M., Wu, J., Harmin, D.A., Laptewicz, M., Barbara-Haley, K., Kuersten, S., et al. (2010). Widespread transcription at neuronal activity-regulated enhancers. Nature *465*, 182–187.

Ku, T., Swaney, J., Park, J.Y., Albanese, A., Murray, E., Cho, J.H., Park, Y.G., Mangena, V., Chen, J., and Chung, K. (2016). Multiplexed and scalable super-resolution imaging of three-dimensional protein localization in size-adjustable tissues. Nat. Biotechnol. *34*, 973–981.

Lassalle, J.M., Bataille, T., and Halley, H. (2000). Reversible inactivation of the hippocampal mossy fiber synapses in mice impairs spatial learning, but neither consolidation nor memory retrieval, in the Morris navigation task. Neurobiol. Learn. Mem. *73*, 243–257.

Lee, I., and Kesner, R.P. (2004a). Differential contributions of dorsal hippocampal subregions to memory acquisition and retrieval in contextual fear-conditioning. Hippocampus *14*, 301–310.

Lee, I., and Kesner, R.P. (2004b). Encoding versus retrieval of spatial memory: double dissociation between the dentate gyrus and the perforant path inputs into CA3 in the dorsal hippocampus. Hippocampus *14*, 66–76.

Lee, K.J., Lee, Y., Rozeboom, A., Lee, J.Y., Udagawa, N., Hoe, H.S., and Pak, D.T. (2011). Requirement for Plk2 in orchestrated ras and rap signaling, homeostatic structural plasticity, and memory. Neuron *69*, 957–973.

Lee, K.J., Queenan, B.N., Rozeboom, A.M., Bellmore, R., Lim, S.T., Vicini, S., and Pak, D.T. (2013). Mossy fiber-CA3 synapses mediate homeostatic plasticity in mature hippocampal neurons. Neuron *77*, 99–114.

Lin, Y., Bloodgood, B.L., Hauser, J.L., Lapan, A.D., Koon, A.C., Kim, T.K., Hu, L.S., Malik, A.N., and Greenberg, M.E. (2008). Activity-dependent regulation of inhibitory synapse development by Npas4. Nature *455*, 1198–1204.

Liu, X., Ramirez, S., Pang, P.T., Puryear, C.B., Govindarajan, A., Deisseroth, K., and Tonegawa, S. (2012). Optogenetic stimulation of a hippocampal engram activates fear memory recall. Nature *484*, 381–385.

Magariños, A.M., Verdugo, J.M., and McEwen, B.S. (1997). Chronic stress alters synaptic terminal structure in hippocampus. Proc. Natl. Acad. Sci. USA *94*, 14002–14008.

Maruo, T., Mandai, K., Takai, Y., and Mori, M. (2016). Activity-dependent alteration of the morphology of a hippocampal giant synapse. Mol. Cell. Neurosci. *71*, 25–33.

Mayford, M., Siegelbaum, S.A., and Kandel, E.R. (2012). Synapses and memory storage. Cold Spring Harb. Perspect. Biol. *4*, a005751.

Nicoll, R.A., and Schmitz, D. (2005). Synaptic plasticity at hippocampal mossy fibre synapses. Nat. Rev. Neurosci. *6*, 863–876.

Pak, D.T., and Sheng, M. (2003). Targeted protein degradation and synapse remodeling by an inducible protein kinase. Science *302*, 1368–1373.

Ramamoorthi, K., Fropf, R., Belfort, G.M., Fitzmaurice, H.L., McKinney, R.M., Neve, R.L., Otto, T., and Lin, Y. (2011). Npas4 regulates a transcriptional program in CA3 required for contextual memory formation. Science *334*, 1669–1675.

Rekart, J.L., Sandoval, C.J., Bermudez-Rattoni, F., and Routtenberg, A. (2007). Remodeling of hippocampal mossy fibers is selectively induced seven days after the acquisition of a spatial but not a cued reference memory task. Learn. Mem. *14*, 416–421.

Ren, D., Navarro, B., Xu, H., Yue, L., Shi, Q., and Clapham, D.E. (2001). A prokaryotic voltage-gated sodium channel. Science *294*, 2372–2375.

Represa, A., and Ben-Ari, Y. (1992a). Kindling is associated with the formation of novel mossy fibre synapses in the CA3 region. Exp. Brain Res. *92*, 69–78.

Represa, A., and Ben-Ari, Y. (1992b). Long-term potentiation and sprouting of mossy fibers produced by brief episodes of hyperactivity. Epilepsy Res. Suppl. *7*, 261–269.

Rios, M., Fan, G., Fekete, C., Kelly, J., Bates, B., Kuehn, R., Lechan, R.M., and Jaenisch, R. (2001). Conditional deletion of brain-derived neurotrophic factor in the postnatal brain leads to obesity and hyperactivity. Mol. Endocrinol. *15*, 1748–1757.

Rolls, E.T. (1996). A theory of hippocampal function in memory. Hippocampus *6*, 601–620.

Ruediger, S., Vittori, C., Bednarek, E., Genoud, C., Strata, P., Sacchetti, B., and Caroni, P. (2011). Learning-related feedforward inhibitory connectivity growth required for memory precision. Nature *473*, 514–518.

Salin, P.A., Scanziani, M., Malenka, R.C., and Nicoll, R.A. (1996). Distinct short-term plasticity at two excitatory synapses in the hippocampus. Proc. Natl. Acad. Sci. USA *93*, 13304–13309.

Sandi, C., Davies, H.A., Cordero, M.I., Rodriguez, J.J., Popov, V.I., and Stewart, M.G. (2003). Rapid reversal of stress induced loss of synapses in CA3 of rat hippocampus following water maze training. Eur. J. Neurosci. *17*, 2447–2456.

Seeburg, D.P., Feliu-Mojer, M., Gaiottino, J., Pak, D.T., and Sheng, M. (2008). Critical role of CDK5 and Polo-like kinase 2 in homeostatic synaptic plasticity during elevated activity. Neuron *58*, 571–583.

Sim, S., Antolin, S., Lin, C.W., Lin, Y., and Lois, C. (2013). Increased cell-intrinsic excitability induces synaptic changes in new neurons in the adult dentate gyrus that require Npas4. J. Neurosci. *33*, 7928–7940.

Sørensen, A.T., Cooper, Y.A., Baratta, M.V., Weng, F.J., Zhang, Y., Ramamoorthi, K., Fropf, R., LaVerriere, E., Xue, J., Young, A., et al. (2016). A robust activity marking system for exploring active neuronal ensembles. eLife *5*, e13918.

Spiegel, I., Mardinly, A.R., Gabel, H.W., Bazinet, J.E., Couch, C.H., Tzeng, C.P., Harmin, D.A., and Greenberg, M.E. (2014). Npas4 regulates excitatory-inhibitory balance within neural circuits through cell-type-specific gene programs. Cell *157*, 1216–1229.

Treves, A., and Rolls, E.T. (1992). Computational constraints suggest the need for two distinct input systems to the hippocampal CA3 network. Hippocampus *2*, 189–199.

Urban, N.N., Henze, D.A., and Barrionuevo, G. (2001). Revisiting the role of the hippocampal mossy fiber synapse. Hippocampus *11*, 408–417.

Vyleta, N.P., Borges-Merjane, C., and Jonas, P. (2016). Plasticity-dependent, full detonation at hippocampal mossy fiber-CA3 pyramidal neuron synapses. eLife *5*, e17977.

Wallace, W., and Bear, M.F. (2004). A morphological correlate of synaptic scaling in visual cortex. J. Neurosci. *24*, 6928–6938.

Wiera, G., and Mozrzymas, J.W. (2015). Extracellular proteolysis in structural and functional plasticity of mossy fiber synapses in hippocampus. Front. Cell. Neurosci. *9*, 427.

Xue, M., Atallah, B.V., and Scanziani, M. (2014). Equalizing excitation-inhibition ratios across visual cortical neurons. Nature *511*, 596–600.

Yoshihara, S., Takahashi, H., Nishimura, N., Kinoshita, M., Asahina, R., Kitsuki, M., Tatsumi, K., Furukawa-Hibi, Y., Hirai, H., Nagai, T., et al. (2014). Npas4 regulates Mdm2 and thus Dcx in experience-dependent dendritic spine development of newborn olfactory bulb interneurons. Cell Rep. *8*, 843–857.

Yue, L., Navarro, B., Ren, D., Ramos, A., and Clapham, D.E. (2002). The cation selectivity filter of the bacterial sodium channel, NaChBac. J. Gen. Physiol. *120*, 845–853.

Yuste, R., and Bonhoeffer, T. (2001). Morphological changes in dendritic spines associated with long-term synaptic plasticity. Annu. Rev. Neurosci. *24*, 1071–1089.

Zhao, S., Studer, D., Chai, X., Graber, W., Brose, N., Nestel, S., Young, C., Rodriguez, E.P., Saetzler, K., and Frotscher, M. (2012a). Structural plasticity of hippocampal mossy fiber synapses as revealed by high-pressure freezing. J. Comp. Neurol. *520*, 2340–2351.

Zhao, S., Studer, D., Chai, X., Graber, W., Brose, N., Nestel, S., Young, C., Rodriguez, E.P., Saetzler, K., and Frotscher, M. (2012b). Structural plasticity of spines at giant mossy fiber synapses. Front. Neural Circuits *6*, 103.

STAR★METHODS

KEY RESOURCES TABLE

REAGENT or RESOURCE	SOURCE	IDENTIFIER
Antibodies		
Rabbit polyclonal anti-Npas4	Lin et al., 2008	N/A
Rat monoclonal anti-flag tag	Thermo Fisher Scientific	RRID: AB_2536846
Mouse monoclonal anti-HA tag	Covance	RRID: AB_2314672
Mouse monoclonal anti-PSD95	Neuromab	RRID: AB_2307331
Guinea pig polyclonal anti-Bassoon	Synaptic System	RRID :AB_2290619
Chicken polyclonal anti-GFP	Thermo Fisher Scientific	RRID: AB_2534023
Rabbit polyclonal anti-RFP	Rockland Antibody & Assays	RRID: AB_2209751
Bacterial and Virus Strains		
pAAV1-hSyn-eGFP	UPenn Vector Core	AV-1-PV1696
pAAV1-hSyn-Cre-eGFP	UPenn Vector Core	AV-1-PV1848
HSV-Npas4-eGFP	Ramamoorthi et al., 2011	N/A
HSV-ΔNpas4-eGFP	Ramamoorthi et al., 2011	N/A
AAV2,8-RAM-d2-tTA-TRE-mKate2	Sørensen et al., 2016	N/A
AAV2,8-ef1a-GFP	Sørensen et al., 2016	N/A
AAV1-hSyn-fDIO-TdTomato	This paper	N/A
AAV1-hSyn-fDIO-GFP-P2A-^{farn}GFP	This paper	N/A
AAV9-ef1a-Flp^{o}	This paper	N/A
AAV9-hSyn-Cre-GFP	This paper	N/A
AAV9-hSyn-ΔCre-GFP	This paper	N/A
AAV1-CaMkII-NaChBac-mKate2	This paper	N/A
AAV1-CaMkII-NaChBac^{mut}-mKate2	This paper	N/A
Chemicals, Peptides, and Recombinant Proteins		
Tetrodotoxin	Tocris	Cat# 1078
Picrotoxin	Tocris	Cat# 1128
DL-AP5 sodium salt	Tocris	Cat# 3693
DNQX disodium salt	Tocris	Cat# 2312
DCG-IV	Tocris	Cat# 0975
LY354740	Tocris	Cat# 3246
WIN55,212-2	National Institute of Mental Health	N/A
Critical Commercial Assays		
RNeasy Mini Kit	QIAGEN	Cat# 74106
Experimental Models: Cell Lines		
Npas4$^{flx/flx}$ hippocampal cultured cells	This paper	N/A
Experimental Models: Organisms/Strains		
Mouse: Npas4$^{-/-}$ (KO)	Lin et al., 2008	N/A
Mouse: Npas4$^{flx/flx}$ (cKO)	Lin et al., 2008	N/A
Nouse: BDNF$^{flx/flx}$	Rios et al., 2001	N/A
Mouse: C57BL/6	Charles River Laboratory	N/A
Oligonucleotides		
Primers Plk2: 5′-AGCAGCGAATGCCTTGAAG-3′, 5′-TCCTCGAAGGACTCTTGCCA-3′	This paper	N/A
Primers Npas4: 5′-CTGCATCTACACTCGCAAGG-3′, 5′-GCCACAATGTCTTCAAGCTCT-3′	This paper	N/A
Primers Tuj1: 5′-CAGTGCGGCAACCAGATAG-3′, 5′-GCAGGTCTGAGTCCCCTACA-3′	This paper	N/A

(*Continued on next page*)

Continued

REAGENT or RESOURCE	SOURCE	IDENTIFIER
Software and Algorithms		
Clampex 10.2	Molecular Devices	N/A
Clampfit 10.2	Molecular Devices	N/A
MiniAnalysis	Synaptosoft	N/A
IgorPro	Wavemetrics	N/A
Prism	GraphPad	N/A
Metamorph	Molecular Devices	N/A
Imaris	Bitplane	N/A
FIJI	NIH	N/A

CONTACT FOR REAGENT AND RESOURCE SHARING

Further information and requests for reagents may be directed to and will be fulfilled by the lead contact, Dr. Yingxi Lin (yingxi@mit.edu).

EXPERIMENTAL MODEL AND SUBJECT DETAILS

Npas4$^{-/-}$ (KO) and Npas4$^{flx/flx}$ mice were generated previously (Lin et al., 2008) and BDNF$^{flx/flx}$ mice (Rios et al., 2001) were generously provided by Dr. Qiang Chang at the University of Wisconsin, Madison. C57BL/6 mice were purchased from Charles River Laboratory. Heterozygous mice were bred to produce Npas4$^{-/-}$ and Npas4$^{+/+}$ littermates, and homozygous mice were bred to produce Npas4$^{flx/flx}$ (cKO) and BDNF$^{flx/flx}$ (BDNF cKO) animals. Mice were weaned at postnatal day 21 and housed by sex in groups of 3-4 until being used for experiments. For CFC, mice were single-housed for 3-5 days prior to conditioning. All mice were housed with a 12 hr light-dark cycle. As standard practice, behavior was done with males, electrophysiology was done with both males and females. Genders of the experimental animals were recorded, but no difference was detected from the data obtained from male and female animals, therefore data were pooled together. No further analysis of gender influence was performed. Rat or mouse pups of either gender were used to produce primary glia or neuron cultures, respectively. Animal protocols were performed in accordance with NIH guidelines and approved by the Massachusetts Institute of Technology and the Albert Einstein College of Medicine Committees on Animal Care.

METHOD DETAILS

Acute Slice Preparation

Npas4$^{-/-}$ mice of either sex, male Npas4$^{flx/flx}$, BDNF$^{flx/flx}$, and C57BL/6 mice were used at 8-10 weeks of age. Mice were anesthetized and decapitated, their brains were removed and immediately immersed in carbogenated (95% O_2, 5% CO_2) ice-cold cutting solution containing (in mM): 105 NMDG, 2.5 KCl, 1.24 NaH_2PO_4, 10 $MgCl_2$, 0.5 $CaCl_2$, 26 $NaHCO_3$, 15 Glucose and 1 Na-ascorbate, 310 mOsm osmolarity, pH adjusted to 7.3 with HCl. Brains were then rapidly blocked and 350μm transverse slices were cut in the same solution using a vibratome (VT1200, Leica). Slices containing dorsal hippocampus were transferred to an incubation chamber filled with warm (32°C) carbogenated cutting solution and moved to room temperature (~23°C) for recovery. Slices were then transferred to a holding chamber filled with carbogenated room temperature ACSF containing (in mM): 119 NaCl, 2.5 KCl, 1.24 NaH_2PO_4, 1.3 $MgCl_2$, 2.5 $CaCl_2$, 26 $NaHCO_3$, and 10 Glucose, 300 mOsm osmolarity, pH 7.3, for storage. Slices were kept in ACSF for at least 1 hr before recording.

Electrophysiology

After recovery, slices were transferred to a recording chamber perfused with carbogenated ACSF at room temperature at a flow rate of 2 mL/min. A borosilicate glass pipette (3-6 MΩ tip resistance) was filled with one of the following internal solutions (in mM). Cs based internal solution for mEPSCs: 130 $CsMeSO_3$, 10 phosphocreatine, 1 $MgCl_2$, 10 HEPES, 0.2 EGTA, 4 Mg-ATP, 0.5 Na-GFP, pH adjusted to 7.25 with CsOH, 290 mOsm osmolarity; high Cl internal solution for mIPSCs: 103 CsCl, 12 $CsMeSO_3$, 5 TEA-Cl, 10 HEPES, 4 Mg-ATP, 0.5 Na-GTP, 0.5 EGTA, 1 $MgCl_2$, pH adjusted to 7.25 with CsOH, 290 mOsm osmolarity. Data were collected using a Multiclamp 700B (Molecular Devices), filtered at 3 kHz and digitized at 10 kHz using a Digidata 1440A and Clampex 10.2 software (Molecular Devices). mEPSCs were recorded in voltage clamp mode and pharmacologically isolated with 0.5 μM tetrodotoxin (TTX, Tocris) and 50 μM picrotoxin (Tocris) in the ACSF. mIPSCs were recorded in voltage clamp mode with 0.5μM TTX, 50μM APV (Tocris) and 20 μM DNQX (Tocris) in the ACSF. To record mEPSCs and mIPSCs, CA3 and CA1 cells were held at −70 mV with a −5 mV pulse delivered every 30-60 s to monitor access resistance. Recordings with access resistance greater than 25 MΩ or changes exceeding 15% were discarded.

In the MFs blockade experiments mEPSCs and mIPSCs were recorded with 1 μM DCG-IV (Tocris) or 300 nM LY354740 (Tocris) in the ACSF. Evoked fEPSPs were recorded with no drugs added to the ACSF. Recording and stimulating pipettes (<2 MΩ tip resistance) were filled with ACSF. Recording pipettes were placed in the stratum lucidum while stimulating pipettes were placed in the DG granule cell layer. Stimulation intensity was adjusted to produce 0.2 – 0.4 mV fEPSP amplitudes. Data were filtered at 1 kHz, digitized at 10 kHz and analyzed with MiniAnalysis (Synaptosoft), Clampfit 10.2 (Molecular Devices) or custom software written in IgorPro (Wavemetrics).

Minimal stimulation of MFs was performed as previously described (Hofmann et al., 2008; Jonas et al., 1993). Briefly, a theta glass-type stimulating pipette was placed in stratum lucidum 50-100 μm away from the recorded CA3 pyramidal cell. Stimulation intensity was set in order to elicit a mossy fiber-derived EPSC and then intensity was reduced until failures were detected. All responses had fast 10%–90% rise time (<2 ms) and were blocked by bath application of 1 μM DCG-IV. To minimize contamination from recurrent associational/commissural (a/c) inputs, AMPAR-EPSC were recorded in presence of the CB1 receptor agonist WIN55,212-2 (5 μM), which selectively reduces the strength of a/c inputs onto CA3 pyramidal cells (Hofmann et al., 2008). The $GABA_A$ receptor antagonist picrotoxin (30 μM) was present in the bath to block fast inhibition. Potency was calculated as the average EPSC amplitude of successful trials while efficacy included both successes and failures. Failure rate was determined as the ratio of failures over total number of trials expressed as percentage.

Experimenters were blind to genotypes or injected viruses. Experimental group sizes were based on generally accepted criteria in the field. Different experimental groups were statistically compared using Mann-Whitney *U*-tests or ANOVA for more than two groups or conditions.

In the case of acute deletion in cKO mice, we inspected every transverse slice, and only animals with viral infection in overall more than 80%–85% of dorsal CA3 and less than 10%–15% dorsal DG were used. In addition, Npas4 cKO animals were excluded if any of their sections indicated Npas4 was deleted in less than 75% of dorsal CA3 and more than 20% of dorsal DG.

Viral Vectors

AAV-hSyn-eGFP and AAV-hSyn-Cre-eGFP were obtained from the University of Pennsylvania Vector Core. HSV-Npas4-eGFP and HSV-ΔNpas4-eGFP were prepared as previously described (Ramamoorthi et al., 2011). HSV-eGFP was obtained from the Viral Gene Transfer Core at MIT. All other AAVs were produced in our lab.

Stereotaxic Injection

Npas4 KO, $Npas4^{flx/flx}$, $BDNF^{flx/flx}$, and C57BL/6 mice were gas-anesthetized with 1.5% isoflurane in O_2 and received bilateral injections of 150-500nl of AAV or 1000nl of HSV into dorsal hippocampal CA3, CA1 or DG. Coordinates for target sites, using bregma as a reference point, were as follows. CA3: AP −1.8, ML ± 2.25, DV −2.35; CA1: AP −2, ML ± 1.5, DV −1.2; DG: AP −1.9, ML ± 1.0, DV −2.1. All injected mice, except in the RAM experiments, were used for recording on post-injection day 3 or 5. GFP and mKate2 expression were verified in acute slices and brains. Mice or tissues with off-target expression were excluded from further analysis.

Only animals with viral infection and effective deletion or overexpression in more than 80%–85% of dorsal CA3 and less than 10%–15% of DG, averaged over all sections, were included in the analysis. Animals were also excluded if any of their sections indicated deletion or overexpression in less than 75% of dorsal CA3 or more than 20% of DG. All experiments and analysis of data were performed in a "blind" manner by investigators that were unaware of the genotype or manipulation.

Sparse Cell Labeling Strategy

To sparsely label cells for morphological analysis, AAV-hSyn-fDIO-TdTomato or AAV-hSyn-fDIO-GFP-P2A-^{farn}GFP was mixed with 1000-2000 diluted AAV-ef1a-Flp^o (final titer ~10^{10} g/mL) and co-injected with other AAVs. For Npas4 acute deletion experiments, AAV-hSyn-fDIO-GFP-P2A-^{farn}GFP+AAV-ef1a-Flp^o mixture was directly injected in DG to sparsely label granule cells and their axon. AAV-hSyn-fDIO-TdTomato + AAV-ef1a-Flpo mixture was co-injected with AAV-hSyn-Cre-GFP or AAV-hSyn-ΔCre-GFP in CA3 to knockdown Npas4 in whole CA3 population but only sparsely label few CA3 cells and their dendritic spines. For RAM morphology experiments, C57BL/6 mice were injected with AAV-RAM-d2-tTA-TRE-mKate2 + low-titer AAV-EF1α-Flp^o + AAV-hSyn-fDIO-GFP-P2A-^{farn}GFP in CA3. For NaChBac experiments, AAV-hSyn-fDIO-GFP-p2a-^{farn}GFP + AAV-ef1a-Flp^o mixture was coinjected with AAV-hSyn-Cre-GFP or AAV-hSyn-ΔCre-GFP + AAV-CaMkII-NaChBac-mKate2 or AAV-CaMkII-$NaChBac^{mut}$-mKate2 to knockdown and manipulate neuronal activity in whole CA3 population but sparsely label few CA3 cells. In both cases, Cre-GFP and ΔCre-GFP expression is restricted to nuclei of CA3 cells, it does not interfere with the dendritic or axonal GFP expression in the lucidum.

Seizure Induction and *In Vivo* Activity Manipulation

For Npas4 deletion verification, Npas4 cKO mice and Npas4 KO mice or their littermates were intraperitoneally (i.p.) injected with kainic acid (Sigma, 12-15 mg/kg dissolved in sterile saline, pH~7.2) to induce visible seizure and processed 2 hr after injection. Mice were used for experiments at 8-10 weeks of age.

Immunohistochemistry

Animals were transcardially perfused with 4% paraformaldehyde (PFA) in phosphate buffered saline (PBS) and brains were post-fixed in 4% PFA at 4°C overnight. Brains were then sectioned at 50 μm or 100 μm thickness using a vibratome. Coronal brain sections

containing hippocampi were blocked in solution containing 1% Triton X-100 and 10% goat serum in PBS for 1 hr at room temperature, then incubated with primary antibody in solution containing 0.1% Triton X-100 and 5% goat serum in PBS overnight at 4°C. Sections were washed in PBS for 10 min 3 times then incubated with secondary antibody in the solution containing 0.1% Triton X-100 and 5% goat serum in PBS at room temperature for 1 hr. Sections were then washed in PBS for 10 min 3 times and mounted on microscope slides with DAPI Fluoromount-G (Southern Biotech) and allowed to dry for at least 2 hr.

Antibodies used: rabbit anti-Npas4 (1:10,000, homemade) (Lin et al., 2008), rat anti-Flag (1:200, Thermo Fisher), mouse anti-HA (1:1,000, Covance), mouse anti-PSD-95 (1:100, NeuroMab), guinea pig anti-Bassoon (1:100, SySy), chicken anti-GFP (1:1,000, Thermos Fisher), rabbit anti-RFP (1:500, Rockland) and Alexa 488, 555, 647 (1:500, Invitrogen).

Stick and Stain

For spine density and TE morphology, we used the "stick-and-stain" protocol as previously described (Wallace and Bear, 2004). Mice were perfused with warm (37°C) 4% PFA in phosphate buffer (PB) and brains were vibratome sectioned into 150 μm slices. Brain slices containing dorsal hippocampi were microinjected in the CA3 region with Alexa Fluor 568 Hydrazide (Invitrogen) using glass pipettes (resistance ~95 MΩ). Slices were submerged in ice-cold PBS and dye propagation was aided by 5 μA current injection through the pipettes. Once cells were filled with dye, slices were post-fixed with 4% PFA overnight. The post-fixed slices were washed 3 times in PBS and mounted or subjected to immunohistochemistry before mounting. After immunohistochemistry or stick-and-stain brain slices containing hippocampi were mounted for image acquisition. Confocal Z series images were acquired using a Fluoview 1000 confocal microscope (Olympus).

SeeDB2

We used the SeeDB2 protocol to quantify structural changes to MF-CA3 synapse morphology. Briefly, brain slices (100 μm) were prepared and then fixed overnight at 4°C with 4% PFA followed by permeabilization with 2% Triton X-100 at room temperature for 12-16 hr. The slices were clarified by soaking them in Omnipaque 350 solution (Sigma, catalog #1344600-200MG) at room temperature for 12 hr as described previously (Ke et al., 2016). Images of cleared slices were recorded by laser Airyscan confocal microscopy (ZEISS LSM 880 with Airyscan). Fifty to seventy optical sections were taken with 63x immersion objective (NA 1.40; WD 0.19 mm, Zeiss).

MAP

In order to quantify changes in synaptic marker densities, we used the MAP protocol as previously described (Ku et al., 2016). Briefly, hippocampi were harvested, embedded in hydrogel, and sliced into 100 μm thick (original thickness) transverse sections, which were then cleared, denatured, and immunostained. MAP-processed hippocampal slices were incubated with primary antibodies in PBS with 0.1% Triton X-100 (PBST) at 37°C overnight, followed by washing at 37°C for 2 hr in PBST three times. The tissue was then incubated with secondary antibodies in PBST at 37°C overnight, followed by washing at 37°C for 2 hr in PBST three times. Antibodies against pre- and post-synaptic markers (Bassoon and PSD-95) were used to label excitatory synapses, and anti-GFP and anti-RFP antibodies were used to replace quenched GFP and tdTomato fluorescent signals. Finally, at least 1 hr before imaging, sections were linearly expanded 4 fold, preserving fine sub-cellular structures and protein localizations. With this expansion, high-resolution confocal z stack imaging of synaptic marker localization was carried out using a Leica TCS SP8 microscope system with 63x, 1.30 NA glycerol-immersion objective (WD 0.3 mm).

2D Spine Density and TE Morphology

For distal spine density measurements, dendritic segments of dye-filled CA3 cells were chosen. Segments were 20 μm in length and at least 30 μm away from the CA3 cell layer. The spine density was calculated as the total spine number per 10 μm. For TE morphology measurements, a proximal dendritic segment was chosen within 30 μm of the soma (lucidum layer). The area of TEs was calculated using Metamorph software (Molecular Devices) by measuring the total area (TEs + dendrites) within the 30 μm length of a Z stack image then subtracting the dendritic area from the total. For each cell, TE density was calculated as the total TE area per total length measured (approximately 30 μm). Experimenters were blind to genotypes or injected viruses. Analyzers were blind to the experimental conditions. Experimental group sizes were based on generally accepted criteria in the field. Different experimental groups were statistically compared using unpaired-Student's t tests or ANOVA for more than two groups or conditions.

3D Reconstruction of MF, TE, and Synaptic Puncta

Reconstruction and analysis of synaptic structures were carried out in Imaris (Bitplane, UK). For morphological analysis of the TE spines and MF terminals, Z stacks were imported and the surface tool was used to generate 3-dimensional dendritic and synaptic structures, which uses an automatic smoothing of the image by application of a Gaussian filter. The volume of individual TE structures was calculated by subtracting the volume of the dendritic shaft, while individual MF terminal volumes can be directly measured from the reconstructions. To quantify synaptic protein density, surface reconstructions of synaptic marker puncta (PSD-95 and Bassoon) was performed using the same creation parameters and the total volume, average puncta volume, and total number of reconstructed puncta was measured from a volume within the stratum lucidum.

Contextual Fear Conditioning

After viral injection, mice were handled to habituate daily for 3 days prior to CFC training. On CFC day 1, mice were placed in a novel chamber, allowed to explore for 58 s and then given a 2 s 0.55 mA footshock. The explore-shock cycle was repeated 3 times and the 4th cycle ended with no shock. After the 4 min training, mice were returned to their home cages. On CFC day 2, mice were returned to the conditioning chamber for 4 min to test memory recall. In experiments with a second recall (Figures 3A and 3B), mice were returned to the chamber for another 4 min 4 days after the first recall (3 days after surgery). Contextual memory was measured by scoring freezing behavior over the 4 min recall period, with freezing defined as the total absence of movement apart from respiration. Scorers were blind to the experimental conditions and experimenters were blind to genotypes or injected viruses. Experimental group sizes were based on generally accepted criteria in the field. Different experimental groups were statistically compared using unpaired-Student's t tests or ANOVA for more than two groups or conditions.

Neuronal Cultures and qRT-PCR

Astrocytes derived from P1-P2 rat cortices were plated at low density in DMEM + 10% FBS in poly-D-lysine-coated 6 well plates and stored and maintained at 37°C in a humidified incubator with 10% CO_2. Once the glial cells had formed a confluent monolayer, approximately 7 days after plating, dissociated hippocampal neurons from mouse Npas4 cKO P0-P1 pups of either sex were plated at a density of 0.5 million cells per well, and the media was changed to NBA supplemented with B27 and Glutamax. Ara-C (5 μM, Sigma) was added to the culture the next day, and conditional media was supplemented with fresh media on DIV7.

For qRT-PCR experiments, hippocampal Npas4-cKO neurons were infected with either AAV-hSyn-GFP-Cre or AAV-hSyn-GFP control virus on DIV9. Cultures were then stimulated with 10 μM kainic acid on DIV15 for up to 9 hr before being lysed in 600 μL Buffer RLT (RNeasy Mini Kit, QIAGEN). Lysates were homogenized using QIAShredder (QIAGEN) and RNA was purified from these lysates using the RNeasy Mini Kit (QIAGEN). Reverse transcription was performed using the SuperScript III First-Strand Synthesis System (Invitrogen), and all samples were then diluted to equalize the amount of RNA used. For qRT-PCR we used 10 μL SsoFast EvaGreen Supermix (Bio-Rad) per reaction, 1 μL of each primer, and 0.7 μL cDNA. Reactions were performed in a Bio-Rad CFX96 real-time PCR detection system using the following protocol: 95°C for 30 s, 45 cycles of 95°C for 5 s and 60°C for 30 s.

RT-PCR Analysis

Analysis was performed using the relative standard curve method, using Tuj1 as the calibration gene for normalization. Primer sequences (forward, reverse) were as follows:

Plk2 (5′-AGCAGCGAATGCCTTGAAG-3′, 5′-TCCTCGAAGGACTCTTGCCA-3′)
Npas4 (5′-CTGCATCTACACTCGCAAGG-3′, 5′-GCCACAATGTCTTCAAGCTCT-3′)
Tuj1 (5′-CAGTGCGGCAACCAGATAG-3′, 5′-GCAGGTCTGAGTCCCCTACA-3′).

To compare gene induction across samples, we then normalized the data for each set of samples to the unstimulated, GFP-infected samples.

QUANTIFICATION AND STATISTICAL ANALYSIS

Data are presented as mean ± SEM unless otherwise stated in text and figure legends. All statistical tests are described in the corresponding figure legends and were performed using Prism (Graphpad). All experiments and analysis of data were performed in a "blind" manner by investigators that were unaware of the genotype or manipulation. In all experiments, "n" indicates the number of cells used. The total number of animals used per experiment is also explicitly reported in the figure legends. Comparisons were done using the Mann-Whitney U test unless otherwise stated. All comparisons are two-sided.